2014

CENTRIFUGATION-BASED ASSAY FOR EXAMINING NANOPARTICLE-LIPID MEMBRANE BINDING AND DISRUPTION

Aihong Xi
University of Rhode Island, xiiona@yahoo.com.sg

CENTRIFUGATION-BASED ASSAY FOR EXAMINING NANOPARTICLE-LIPID MEMBRANE BINDING AND DISRUPTION

BY

AIHONG XI

A THESIS SUBMITTED IN PARTIAL FULFILLMENT OF THE REQUIREMENTS FOR THE DEGREE OF

MASTER OF SCIENCE

IN

CHEMICAL ENGINEERING

UNIVERSITY OF RHODE ISLAND

2014

MASTER OF SCIENCE THESIS

OF

AIHONG XI

APPROVED:

Thesis Committee:

Major Professor Geoffrey D. Bothun

Mercedes A. Rivero-Hudec

Jason R. Dwyer

Nasser H. Zawia
DEAN OF THE GRADUATE SCHOOL

UNIVERSITY OF RHODE ISLAND
2014

ABSTRACT

Physical disruption of cellular membranes arising from interactions with engineered nanoparticles is an important, but poorly understood aspect of nanotoxicology and nanomedicine. Model cellular membranes (i.e. lipid bilayers) can be used to identify interaction mechanisms, and most studies have largely focused on lipid bilayers supported on solid planar or spherical substrates. While useful and informative, these systems do not accurately represent an intact cell membrane because they restrict the elastic motion of the bilayer and the capacity for mechanical changes. Free standing bilayers are preferred, but add complexity. Given the importance of nanoparticle–membrane interactions in nanotoxicology and nanomedicine, and the vast range in nanoparticle composition, size, shape, and surface functionalization, there is a need to develop techniques that can rapidly and inexpensively analyze the membrane-nanoparticle activity by using free standing or unsupported membranes.

This work develops a centrifugation-based assay that can analyze the membrane- nanoparticle activity as a function of nanoparticle surface functionalization, membrane lipid composition, and monovalent salt concentration (NaCl). Free standing, unsupported vesicles were used to gain relevant information on elastic membrane deformation and vesicle destabilization due to nanoparticle binding. Silver nanoparticles were chosen due to their widespread biological applications and surface plasmon resonance (SPR) properties. UV-vis based centrifugation assay, coupled with cryo-TEM and DLS analysis, was proposed to screen nanoparticle-membrane interactions; silver nanoparticles binding ratio R_{SPR} was calculated as a function of Ag nanoparticle coating and vesicle composition. Study showed that strong electrostatic

attraction led to significant sedimentation, vesicle / membrane disruption and higher R_{SPR} value; in contrast, systems that exhibited weak or no electrostatic attraction did not show significant sedimentation, membrane disruption or high R_{SPR} value. The centrifugation assay provides a rapid and straightforward way to screen nanoparticle–membrane interactions.

ACKNOWLEDGMENTS

I like to express my appreciation with deep gratitude to the following people for their contributions:

- To Professor Geoffrey D. Bothun for his extraordinary teaching and mentoring. Dr. Bothun has brought me to the area of nanotoxicology and nanomedicine, and guided me to form base foundation, and taught me critical thinking and academic writing. Dr. Bothun has demonstrated great passion and commitment to research and teaching. My gratitude goes to Dr. Bothun's wife, Amy J. Bothun, for her friendship and encouragement.
- To Professor Michael Greenfield for his extremely attentive assistance and fun teaching.
- To Dr. Richard Kingsley for his assistance with cryo-TEM imaging.
- To my committee, Dr. Mercedes A. Rivero-Hudec, Dr. Jason R. Dwyer, Dr. Vinka Oyanedel-Craver, for their time and effort.
- To Bothun Group, Dr Chen, Dr Gupta, Dr Kurniawan, Matthew Preiss, Chris Bobba, Sara Field, Maximilian Sender and Yaser Kashcooli, for their honest feedback, kind cooperation and fun time.
- To Brenda Moyer, Sheryl Girard, for their helpful reminders and facilitation.
- To Department of Chemical Engineering of University of Rhode Island, for providing me opportunity to study for my Master degree.
- To my families and friends, for their unconditional love, support and inspiration.

PREFACE

Manuscript format was used to prepare this dissertation.

Chapter 3 was originally published by A. Xi and G.D. Bothun, Analyst, 2014, 139, 973-981. In addition to the published manuscript, supporting figures have been included.

TABLE OF CONTENTS

LIST OF TABLES

LIST OF FIGURES

FIGURE PAGE

CHAPTER 1

Introduction

1.1 Nanoparticle - membrane interaction

Over the past two decades, nanoparticles have been increasingly used for biological applications such as antimicrobial agents, therapeutics imaging, diagnosis and targeted drug / gene delivery.[1-33] For example, silver nanoparticles have been used for disinfection and creating antifouling surfaces.[22] Superparamagnetic iron oxide (SPIO) and gold (Au) nanoparticles have been reported in the field of tumor disgnostics and cancer treatment.[9-10, 16-21] Semiconducting nanocrystals, e.g. quantum dots, were used to improve biological imaging for medical diagnostics,[14] and these crystals were able to offer resolutions up to 1,000 times better than conventional dyes used in many biological tests. Furthermore, multifunctional nanoparticles, which have both diagnostic and therapeutic functions, are able to stimulate gene or drug release at targeted location when triggered by external stimuli, and minimize the risk to normal tissues.[26-30]

The introduction of nanoparticles into biological processes leads to new challenges: (1) the characterization of the interaction between nanoparticles and cell membranes; (2) the evaluation of biocompatibility between nanoparticles and cell membranes; (3) the measurement of the cytotoxicity induced by nanoparticles and (4) the prediction of the impact of nanoparticles to biological systems. It has been observed that nanoparticles were able to bind to membrane, causing local changes in membrane

curvature.[34-37] The extent of nanoparticle-induced biophysical and/or biochemical changes on cell membranes would be dependent on the size, charge, surface reactivity, surface chemistry and compositions of nanoparticles.[38-42] It has been studied that nanoparticles may introduce carcinogenic risks, which may be triggered by the production of reactive oxygen species (ROS) by macrophages attempting to destroy foreign materials on the inflammation sites. The ROS produced in this process, may cause DNA damage as well as inflammatory lesions associated with carcinogenesis.[43-44]

The broad applications of nanoparticles and their toxicity prompt investigations not only on their functional mechanisms, but also on their cytotoxicity. The size, charge, surface chemistry, and compositions of nanoparticles are important parameters for their physicochemical properties and biological applications. Therefore, there is the urgency to determine how the size, charge, and surface chemistry of nanoparticles influence their functional mechanism and their cytotoxicity.[45-47] In this study, nanoparticle - membrane interaction was characterized in order to provide fundamental understanding of the interaction between nanoparticles and cellular systems, and to provide guidance in the design and development of safe nanoparticles for biological applications.

1.2 Silver nanoparticle - membrane interaction

In this work, silver nanoparticles (AgNPs) were chosen to study the nanoparticle membrane interaction due to their widespread biological applications and surface plasmon resonance (SPR) property. Firstly, silver nanoparticles are important antimicrobial agents.[48-52] AgNPs are able to destroy bacterial cell walls, to trigger

conformational changes of the ion channel, to cause changes of channel opening and dysfunctions. Therefore understanding silver nanoparticle - membrane interactions is essential to understand their toxic effects on both human health and the environment. Secondly, when silver nanoparticles interact with light, the conduction electrons on the silver surface oscillates at specific wavelength, giving AgNPs the surface plasmon resonance (SPR) property.[53-54] SPR can be assessed by ultraviolet-visible (UV-vis) spectroscopy. Its absorbance and wavelength are functions of AgNP concentrations and aggregation states. Therefore, SPR allows the determination of both AgNP concentrations in supernatant and sediment phases, and AgNP aggregation states in solution and after membrane binding.

Experiments were conducted using anionic, cationic and neutral silver nanoparticles and lipid bilayer vesicles. Unsupported vesicles were used to allow elastic membrane deformation and vesicle destabilization due to nanoparticle binding. Supernatant and sediment phases were characterized by cryogenic transmission electron microscopy (cryo-TEM) to directly image nanoparticle membrane binding and to connect vesicle stability and structure with the observed centrifugation behavior.

1.3 Specific Research Aim and Hypothesis

Aim: Determine nanoparticle - membrane interactions; quantify electrostatic interactions as a function of nanoparticle size, surface chemistry and membrane composition; examine the degree of nanoparticle aggregation at membrane / water interfaces; and the effects of aggregation on membrane disruption.

Hypothesis: Nanoparticle - membrane interactions lead to nanoparticle aggregation at membrane / water interfaces, and cause membrane disruption and pore formation. These phenomena can be examined by employing a centrifugation-based assay.

Task 1. *Develop a centrifugation-based assay capable of screening nanoparticle-membrane binding.*

Task 2. *Determine the extent of nanoparticle aggregation as a function of nanoparticle-membrane and nanoparticle-nanoparticle interactions via UV-vis spectroscopy.*

Task 3. *Examine membrane disruption and destabilization due to nanoparticle binding and aggregation via cryo-TEM.*

REFERENCE

1 http://www.nano.gov/

2 Michel, R., Gradzielski, M., Experimental Aspects of Colloidal Interactions in Mixed Systems of Liposome and Inorganic Nanoparticle and Their Applications, Int. J. Mol. Sci. 13, 2012, 11610-11642

3 Elsaesser, A., Howard C.V., Toxicology of nanoparticles, Advanced Drug Delivery Reviews 64 2012, 129–137

4 Carr, K.E., Smythb, S.H., McCullough, M.T., Morris, J.F., Moyes, S.M., Morphological aspects of interactions between microparticles and mammalian cells: intestinal uptake and onward movement, Progress in Histochemistry and Cytochemistry 46, 2012, 185–252

5 Schulz, M., Olubummo, A., and Binder, W.H., Beyond the lipid-bilayer: interaction of polymers and nanoparticles with membranes, Soft Matter, 8, 2012, 4849–4864

6 Lai, Z.W., Yan, Y., Caruso, F., Nice, E.C., Emerging Techniques in Proteomics for Probing Nano-Bio Interactions, VOL. 6 NO. 12, 2012, 10438–10448

7 Li, Y., Chen, Z.W., Gu, N., *In vitro* biological effects of magnetic nanoparticles, 2012 Vol.57 No.31 3972-3978

8 Mahmoudi, M., Lynch, I., Ejtehadi, M. R., Monopoli, M. P., Bombelli, F. B., Laurent, S., Protein Nanoparticle Interactions: Opportunities and Challenges, Chem. Rev. 111, 2011, 5610–5637

9 Ojea-Jime´nez, I., Garcı´a-Ferna´ndez, L., Lorenzo, J., Puntes, V.F., Facile Preparation of Cationic Gold Nanoparticle-Bioconjugates for Cell Penetration and Nuclear Targeting, ACS Nano VOL. 6, NO. 9, 2012, 7692–7702

10 Rasch, M.R., Rossinyol, E., Korgel, B.A., Hueso, J. L., Goodfellow, B.W. and Arbiol, J., Hydrophobic Gold Nanoparticle Self-Assembly with Phosphatidylcholine Lipid: Membrane-Loaded and Janus Vesicles Nano Lett. 10, 2010, 3733–3739

11 Bihan, O. L., Bonnafous, P., Marak, L., Bickel, T., Trépout, S., Mornet, S., Felix De Haas, F. D., Talbot, H., Taveau, J. C., Lambert, O., Cryo-electron tomography of nanoparticle transmigration into liposome, Journal of Structural Biology 168, 2009, 419–425

12 Yang, J. A., Phan, H. T., Shruti Vaidya, S., Murphy, C. J., Nanovacuums: Nanoparticle Uptake and Differential Cellular Migration on a Carpet of Nanoparticles, Nano Lett. 13, 2013, 2295−2302

13 Sabuncua, A.C., Grubbsb, J., Qiana, S., Abdel-Fattahc, T.M., Staceyb, M.W. and Beskoka, A., Probing nanoparticle interactions in cell culture media, Colloids and Surfaces B: Biointerfaces 95 (2012) 96– 102

14 Kang, H.G., Tokumasu, F., Clarke, M., Zhou, Z., Tang, J., Nguyen, T., Probing dynamic fluorescence properties of single and clustered quantum dots toward quantitative biomedical imaging of cells, Wiley Interdiscip. Rev. Nanomed. Nanobiotechnol. 2 (2010) 48.

15 Kang, B., Mackey, M.A., El-Sayed, M.A., Nuclear targeting of gold nanoparticles in cancer cells induces DNA damage, causing cytokinesis arrest and apoptosis, J. Am. Chem. Soc. 132 (2010) 1517.

16 Yallapu, M.M., Foy, S.P., Jain, T.K., Labhasetwar, V., Curcumin-loaded magnetic nanoparticles for breast cancer therapeutics and imaging applications. Pharmacol. Res. 27 (2010) 2283.

17 Ghosh, P. S.; Kim, C.-K.; Han, G.; Forbes, N. S.; Rotello, V. M., Efficient Gene Delivery Vectors by Tuning the Surface Charge Density of Amino Acid Functionalized Gold Nanoparticles, ACS Nano 2008, 2, 2213–2218.

18 Daniel, M.-C., Astruc, D., Gold nanoparticles: assembly, supramolecular chemistry, quantum-size-related properties, and applications toward biology, catalysis, and nanotechnology, Chemical Reviews 104 (2004) 293–346.

19 Lévy, R., Shaheen, U., Cesbron, Y. and Sée, V., Gold nanoparticles delivery in mammalian live cells: a critical review, Nano Reviews 1 (2010).

20 Eustis, S. and El-Sayed, M.A., Why gold nanoparticles are more precious than pretty gold: Noble metal surface plasmon resonance and its enhancement of the radiative and nonradiative properties of nanocrystals of different shapes, Chemical Society Reviews 35 (2006) 209–217.

21 Li, Y., Chen, Z.W., Gu, N., *In vitro* biological effects of magnetic nanoparticles, 2012 Vol.57 No.31 3972-3978

22 Ahamed, M., AlSalhi, M.S., Siddiqui, M.K.J., Silver nanoparticle applications and human health, Clinica Chimica Acta 411, 2010, 1841–1848

23 Rosi, N. L.; Mirkin, C. A. Nanostructures in biodiagnostics. Chem. Rev. 2005, 105, 1547–1562.

24 Giljohann, D. A.; Mirkin, C. A. Drivers of biodiagnostic development. Nature 2009, 462, 461–464.

25 Peer, D.; Karp, J. M.; Hong, S.; FaroKhzad, O. C.; Margalit, R.; Langer, R. Nanocarriers as an emerging platform for cancer therapy. Nat. Nanotechnol. 2007, 2, 751–760.

26 Lammers, T.; Aime, S.; Hennink, W. E.; Storm, G.; Kiessling, F. Theranostic nanomedicine. Acc. Chem. Res. 2011, 44, 1029–1038.

27 Tassa, C.; Shaw, S. Y.; Weissleder, R. Dextran-coated iron oxide nanoparticles: a versatile platform for targeted molecular imaging, molecular diagnostics, and therapy. Acc. Chem.Res. 2011, 44, 842–852.

28 Girard, P. P.; Cavalcanti-Adam, E. A.; Kemkemer, R.; Spatz, J. P. Cellular chemomechanics at interfaces: sensing, integration and response. Soft Matter 2007, 3, 307–326.

29 Chen, X. D.; Lenhert, S.; Hirtz, M.; Lu, N.; Fuchs, H.; Chi, L. F. Langmuir-Blodgett patterning: A bottom-up way to build mesostructures over large areas. Acc. Chem. Res. 2007, 40, 393–401.

30 Cevc, G. Lipid vesicles and other colloids as drug carriers on the skin. Adv. Drug Deliv. Rev. 2004, 56, 675–711.

31 Leckband, D., Israelachvili, J., Intermolecular forces in biology, Quarterly Reviews of Biophysics 34, 2, 2001, 105–267

32 Mouritsen, O. G., Lipidology and lipidomics—quo vadis? A new era for the physical chemistry of lipids, Phys. Chem. Chem. Phys., 2011, 13, 19195–19205

33 Nagle, J. F., Tristram-Nagle, S., Structure of lipid bilayers, Biochimica et Biophysica Acta, 2000, 1469, 159-195

34 Sperling, R. A.; Rivera Gil, P.; Zhang, F.; Zanella, M.; Parak, W. J. Biological Applications of Gold Nanoparticles. Chem. Soc. Rev. 2008, 37, 1896–1908.

35 Chithrani, B. D.; Ghazani, A. A.; Chan, W. C. W. Determining the Size and Shape Dependence of Gold Nanoparticle Uptake into Mammalian Cells. Nano Lett. 2006, 6, 662–668.

36 Boisselier, E.; Astruc, D. Gold Nanoparticles in Nanomedicine: Preparations, Imaging, Diagnostics, Therapies and Toxicity. Chem. Soc. Rev. 2009, 38, 1759–1782.

37 Verma, A.; Stellacci, F. Effect of Surface Properties on Nanoparticle Cell Interactions. Small 2010, 6, 12–21.

38 Lewinski, N., Colvin, V., Drezek, R., Cytotoxicity of nanoparticles, Small 4 (2008) 26.

39 Hussain, S.M., Braydich-Stolle, L.K., Schrand, A.M., Murdock, R.C., Yu , K.O., Mattie, D.M., Toxicity evaluation for safe use of nanomaterials: recent achievements and technical challenges, Adv. Mater. 21 (2009) 1549.

40 Maurer-Jones, M.A., Bantz, K.C., Love, S.A., Marquis, B.J., Haynes, C.L. , Toxicity of therapeutic nanoparticlesNanomedicine (Lond.) 4 (2009) 219.

41 Pelley, J.L., Daar, A.S., Saner, M.A., State of academic knowledge on toxicity and biological fate of quantum dots, Toxicol. Sci. 112 (2009) 276.

42 Kunzmann, A., Andersson, B., Thurnherr, T., Krug, H.; Scheynius, A. and Fadeel, B. Toxicology of engineered nanomaterials: Focus on biocompatibility, biodistribution and biodegradation. Biochim. Biophys. Acta 2011, 1810, 361–373.

43 Ishida, T. and Kiwada, H., Accelerated blood clearance (ABC) phenomenon upon repeated injection of PEGylated liposomes. Int. J. Pharm. 2008, 354, 56–62.

44 Loo, S. C. J., Moore, T., Banik, B. and Alexis, F., Biomedical Applications of Hydroxyapatite Nanoparticles. Curr. Pharm. Biotechnol. 2010, 11, 333–342.

45 Zhao, F., Zhao, Y., Liu, Y., Chang, X., Chen, C. and Zhao, Y., Cellular uptake, intracellular trafficking, and cytotoxicity of nanomaterials. Small 2011, 7, 1322–1337.

46 Soenen, S. J., Rivera-Gil, P., Montenegro, J.-M., Parak, W. J., De Smedt, S. C. and Braeckmans, K., Cellular toxicity of inorganic nanoparticles: Common aspects and guidelines for improved nanotoxicity evaluation. Nano Today 2011, 6, 446–465.

47 Binder, W.H., Barragan, V. and Menger, F.M., Domains and Rafts in Lipid Membranes, Angew.Chem. Int. Ed. 2003, 42, 5802-5827.

48 Ahamed, M., AlSalhi, M.S. and Siddiqui, M.K.J., Silver nanoparticle applications and human health, Clinica Chimica Acta 411, 2010, 1841–1848

49 Ostad, S.N., Dehnad, S., Nazari, Z.E., Fini, S.T., Mokhtari, N., Shakibaie,M. and Shahverdi, A.R., Cytotoxic Activities of Silver Nanoparticles and Silver Ions in Parent and Tamoxifen-Resistant T47D Human Breast Cancer Cells and Their Combination Effects with Tamoxifen against Resistant Cells, Avicenna J Med Biotechnol. Oct-Dec; 2(4): 2010, 187–196

50 Xiu, Z.M., Zhang, Q.B., Puppala, H.L., Colvin, V.L., Alvarez, P.J.J., Negligible Particle-Specific Antibacterial Activity of Silver Nanoparticles, Nano Lett. 12, 2012, 4271−4275

51 Lansdown, A.B.G., A Pharmacological and Toxicological Profile of Silver as an Antimicrobial Agent in Medical Devices, Adv. Pharmacol. Sci. 2010, 910-916

52 Zook, J.M., Long, S.E., Cleveland, D., Geronimo, C.L.A. and MacCuspie, R.I., Measuring Silver Nanoparticle Dissolution in Complex Biological and Environmental Matrices Using UV-Visible, Absorbance. Anal. Bioanal. Chem. 401, 2011, 1993–2002

53 Li, W.R.; Xie, X.B.; Shi, Q.S., Duan, S.S., OuYang, Y.S., Chen, Y.B., Biometals 24, 2011, 135–141

54 Lubick, N., Nanosilver toxicity: ions, nanoparticles or both? Environ. Sci. Technol., 42 (23), 2008, 8617–8617

CHAPTER 2

Background

2.1 Cell membranes (vesicles / lipid bilayers)

Membranes are the most common cellular structure in both animals and plants (Figure 2-1).[1-3] Membranes participate almost all aspects of cellular activity, which ranges from simple mechanical functions such as motility, food entrapments, and transport, to highly specific biochemical processes such as energy transduction, immunological recognition, nerve conduction and biosynthesis.

Lipids are major components of all cell membranes. Most biological lipids are phospholipids or glycolipids that generally consist of hydrophilic heads and hydrophobic tails (Figure 2-1). When lipids contact with water, 'heads' are attracted to water, while the hydrophobic acyl 'tails' are repelled by water, forming lipid bilayer shells that are 4 - 5 nm thick with an aqueous core.[1-3] Other than protecting the cell, the lipid bilayer is able to compartmentalize different regions on a cell membrane. Antibodies, protein receptors, and other biosensor molecules that are attached to the lipid bilayers are able to accommodate enzymes, proteins, DNA, and various drug molecules. Simply, lipids act as a solvent for all the substances, facilitating their diffusion through the membrane.

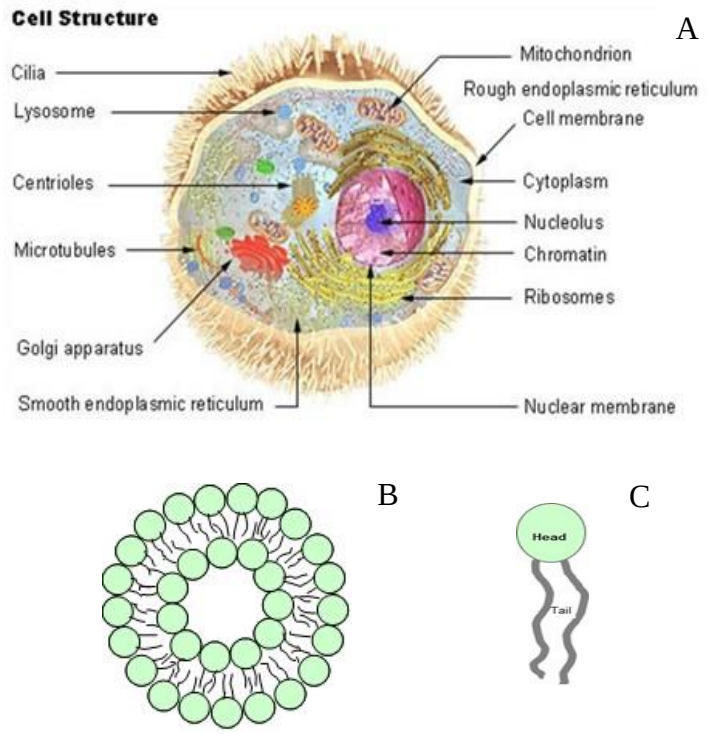

Figure 2-1 (A) Cell structure and cell membrane (*wikipedia*). (B) Schematic depicting lipid bilayer (also called vesicles). (C) A single lipid structure.

Vesicles are artificially formed capsules of phospholipid bilayers, and able to store and carry hydrophobic molecules to move within their bilayer, or hydrophilic molecules in their inner shell, which forms a very flexible carrier systems. It is frequent to find vesicles in cosmetic and pharmaceutical formulations.[2] Vesicles serve as model systems for experimental and theoretical studies on the characterization of the interaction between nanoparticles and cell membrane.

Table 2-1. Membrane lipids used in this study.

Lipid	Acyl tail	T_m (°C)[a]
1,2-dipalmitoyl-sn-glycero-3-phosphocholine (DPPC)	16:0	41
1,2-dipalmitoylphospho-rac-1-g-sn-glycero-3-lycerol (sodium salt) (DPPG)	16:0	41
1,2-dipalmitoyl-3-trimethylammonium-propane (chloride salt) (DPTAP)	16:0	41

[a]Lipid gel to fluid main phase transition or melting temperature.

Phospholipid bilayers in vesicles exhibit a sharp phase transition at specified temperatures,[1-3] which is a very important characteristics in their molecular organization. During the phase transition, a solid ordered phase transforms to a high-temperature liquid-disorder phase. The phase transition is attributed to the melting of their hydrocarbon acyl chains. Below the chain melting temperature (T_m), the hydrocarbon chains of phospholipid molecules are tightly bounded together by the van der Waals forces, and the vesicles exist in a solid state-like gel phase, leading to the appearance of characteristic angular shapes in vesicles. On the other hand, at temperatures above T_m, the hydrocarbon chains of phospholipid molecules exhibit lateral as well as inter-layer mobility, and the vesicles exist in a fluid phase. The phase transition temperatures of lipids used in this study are listed in Table 2-1.

2.2 Experimental techniques

For the biomedical applications of nanoparticles, it is necessary to understand cell membrane-nanoparticle interactions and to assess the safety of nanomaterials. membrane-nanoparticle interaction studies are complicated [4-13] by (1) the considerable variation in types of nanoparticles, NP surface functionalization, physicochemical parameters of the nanoparticles (size, charge, shape and surface area) and nanoparticle concentration; (2) the lipid composition and the types of assay used; (3) unconfirmed scientific basis for cytotoxicity; and (4) the lack of characterization techniques. Therefore, a variety of experimental techniques has been used to understand the interaction mechanism and the nanoparticle-induced cytotoxicity to guide the design of biocompatible nanomaterials.

Differential scanning calorimetry (DSC) is capable of capturing the phase transition behaviors of vesicles such as the transition temperatures (T_m), T_m shifts, and DSC curve shape changes when vesicles interact with nanoparticles. For example, during their interactions with cell membranes, superparamagnetic iron oxide (SPIO) nanoparticles at 30 nm show more significant T_m shifts compared to SPIO at 16 nm.[14] A decrease of T_m and a broadening of the transition were observed on supported bilayers which were formed on the 100 nm silica beads.[15]

Atomic force microscopy (AFM) was developed to quantitatively measure the binding force of nanoparticles with cell membranes and to study the morphological changes of the membranes due to their interaction with nanoparticles. For example, through AFM studies, it was found that electrostatic interaction drives the binding of nanoparticles to membranes which causes membrane disruption.[16-17] AFM study by

Roiter et al.[18] indicated that nanoscale pores were formed on the lipid bilayer when the diameter of nanoparticle was smaller than 22 nm. Furthermore, nanoparticles would be enveloped by the lipid bilayers when the diameter was larger than 22 nm.

Quartz crystal microbalance with dissipation (QCM-D) has been a popular method recently because it is sensitive to frequency changes (Δf) and energy dissipation (ΔD) when nanoparticles bind to membrane.[19-22] Inductively coupled plasma optical emission spectrometry (ICP-OES) or mass spectrometry (MS) has also been used, for example, to probe the interaction between functionalized Au nanoparticles and silica sphere-supported lipid membranes (SSLMs) by measuring the concentrations of Au nanoparticles both in the aqueous electrolytes (supernatant) and in/on the lipid bilayers.[23]

The electrophysiological approach[24] coupled with the droplet-in-oil methodology has been employed to study the interaction between nanoparticles and cell membranes. In the report by De Palnque et al., the droplet-in-oil methodology was first used to create lipid bilayers through the self-assembly of two water droplets coated with a lipid monolayer at water-oil interface. Subsequently, it was found that when silica nanospheres covered as low as 0.02% of the surface of the bilayers, the electrophysiological approach was able to detect bilayer current change caused by nanoparticle adsorption to lipid bilayers. Another electrical approach[25] quantified nanoparticle adsorption to membrane by detecting capacitive increase of suspended planar lipid bilayers.

In addition, in recent years, computer simulation is gaining increasing attention for the study of nanoparticle-membrane interactions.[26-30] These studies have also

provided critical information on the relationships between the interactions and the composition, geometry, and physicochemical properties of the nanoparticles.

2.3 Centrifugation-based assays

For decades researchers have utilized centrifugation-based assays to determine protein membrane affinity or binding, where the amount of bound protein can be determined by a mass balance taking into account the supernatant (free protein) and sediment (membrane-bound protein) phases.[31] Centrifugation methods to assay protein-membrane binding affinity have proven to be simple and inexpensive techniques. Proteins are one of nature's nanoparticles, and the objective of this work is to test the applicability of a centrifugation-based assay for quantifying physical nanoparticle-membrane interactions in model bacterial membranes and to examine electrostatic interactions as a function of nanoparticle size and surface chemistry and membrane composition, and to determine how local interactions yield global changes in membrane structure and function.

Reference

1 Nagle, J. F., Tristram-Nagle, S., Structure of lipid bilayers, Biochimica et Biophysica Acta, 2000, 1469, 159-195.

2 Cevc, G., Lipid vesicles and other colloids as drug carriers on the skin. Adv. Drug Deliv. Rev. 2004, 56, 675–711.

3 Mouritsen, O. G., Lipidology and lipidomics—quo vadis? A new era for the physical chemistry of lipids, Phys. Chem. Chem. Phys., 2011, 13, 19195–19205

4 Mahmoudi, M., Azadmanesh, K., Shokrgozar, M. A., Journeay, W. S., Laurent, S., Effect of nanoparticles on the cell life cycle, Chem. Rev. 2011, 111, 3407.

5 Fadeel, B., Garcia-Bennett, A. E., Better safe than sorry: understanding the toxicological properties of inorganic nanoparticles manufactured for biomedical applications, Adv. Drug Delivery Rev. 2010, 62, 362.

6 Soenen, S.J., De Cuyper, M., Assessing iron oxide nanoparticle toxicity in vitro: current status and future prospects, Nanomedicine (Lond.) 5 (2010) 1261.

7 Clift, M.J.D., Boyles, M.S.P., Brown, D.M., Stone, V., An investigation into the potential for different surface-coated quantum dots to cause oxidative stress and affect macrophage cell signalling in vitro, Nanotoxicology 4 (2010) 139.

8 Thanh, N.T.K., Green, L.A.W., Functionalisation of nanoparticles for biomedical applications, Nano Today 5 (2010) 213.

9 Verma, A., Stellacci, F., Effect of surface properties on nanoparticle–cell interactions, Small 6 (2010) 12.

10 Mironava, T., Hadjiargyrou, M., Simon, M., Jurukovski, V., Rafailovich, M.H., Gold nanoparticles cellular toxicity and recovery: effect of size, concentration and exposure time, Nanotoxicology 4 (2010) 120.

11 Lanone, S., Rogerieux, Geys, F., J., Dupont, A., Maillot-Marechal, E., Boczkowski, J., Comparative toxicity of 24 manufactured nanoparticles in human alveolar epithelial and macrophage cell linesPart. Fibre Toxicol. 6 (2009) 14.

12 Monteiro-Riviere, N.A., Inman, A.O., Zhang, L.W., Limitations and relative utility of screening assays to assess engineered nanoparticle toxicity in a human cell line, Toxicol. Appl. Pharmacol. 234 (2009) 222.

13 Pfaller, T., Colognato, R., Nelissen, I., Favilli, F., Casals, E., Ooms, D., The suitability of different cellular in vitro immunotoxicity and genotoxicity methods for the analysis of nanoparticle-induced events, Nanotoxicology 4 (2010) 52.

14 Chen, Y.J., Bothun, G.D., Cationic Gel-Phase Liposomes with "Decorated"Anionic SPIO Nanoparticles: Morphology, Colloidal, and Bilayer Properties. Langmuir 27, 2011, 8645–8652

15 Ahmed, S., Wunder, S.L., Effect of High Surface Curvature on the Main Phase Transition of Supported Phospholipid Bilayers on SiO2 Nanoparticles. Langmuir 25, 2009, 3682–3691

16 Vasir, J.K., Labhasetwar, V., Quantification of the force of nanoparticle-cell membrane interactions and its influence on intracellular trafficking of nanoparticles, Biomaterials 29, 2008, 4244–4252

17 Xiao, X.Y., Montaño, G.A., Edwards, T. L., Allen, A., Achyuthan, K.E., Polsky, R., Wheeler, D.R., and Brozik, S.M., Surface Charge Dependent Nanoparticle Disruption and Deposition of Lipid Bilayer Assemblies, Langmuir 28, 2012, 17396−17403

18 Roiter, Y., Ornatska, M., Rammohan, A.R., Balakrishnan, J., Heine, D.R., Minko, S., Interaction of nanoparticles with lipid membrane. Nano Letters 8(3) (2008) 941-944.

19 Frost, R., Jönsson, G. E., Chakarov, D., Svedhem, S., Kasemo, B., Graphene Oxide and Lipid Membranes: Interactions and Nanocomposite Structures, Nano Lett. 2012, 12, 3356−3362

20 Reimhult, E., Za¨ch, M., Ho¨o¨k, F., Kasemo, B., A Multitechnique Study of Liposome Adsorption on Au and Lipid Bilayer Formation on S_iO_2, Langmuir 2006, 22, 3313-3319

21 Wang, K.F., Nagarajan, R., Mello, C.M., and Camesano, T.A., Characterization of Supported Lipid Bilayer Disruption By Chrysophsin-3 Using QCM-D, J. Phys. Chem. B 115, 2011, 15228–15235

22 Eriksson, A.I.K., Edwards, K., Hagfeldt, A., and Hernańdez V.A., Physicochemical Characterization of Phosphopeptide/Titanium Dioxide Interactions Employing the Quartz Crystal Microbalance Technique, J. Phys. Chem. B 117, 2013, 2019−2025

23 Hou, W.C., Moghadam, B.Y., Corredor, C., Westerhoff, P., Posner, J.D., Distribution of Functionalized Gold Nanoparticles between Water and Lipid Bilayers as Model Cell Membranes, Environ. Sci. Technol. 46, 2012, 1869−1876

24 De Planque, M.R.R., Aghdaei, S., Roose, T., Morgan, H., Electrophysiological Characterization of Membrane Disruption by Nanoparticles, ACS Nano, VOL. 5 NO. 5, 2011, 3599-3606

25 Carney, R.P., Astier, Y., Carney, T.M., Voı̈tchovsky, K., Paulo H. Jacob Silva, P.H., Stellacci, F., Electrical Method to Quantify Nanoparticle Interaction with Lipid Bilayers, ACS nano, VOL. 7 , NO. 2, 2013, 932–942

26 Pogodin, S., Werner, M., Sommer, J.U., Baulin, V.A., Nanoparticle-Induced Permeability of Lipid Membranes, ACS Nano 2012 VOL. 6 NO. 12, 2012, 10555–10561

27 Nangia, S., Sureshkumar, R., Effects of Nanoparticle Charge and Shape Anisotropy on Translocation through Cell Membranes, Langmuir 28, 2012, 17666−17671

28 Ding, H., Tian, W., Ma, Y., Designing Nanoparticle Translocation through Membranes by Computer Simulations, ACS Nano, VOL. 6 NO. 2, 2012, 1230–1238

29 Ruiz-Herrero, T., Velasco, E., Hagan, M.F., Mechanisms of Budding of Nanoscale Particles through Lipid Bilayers, J. Phys. Chem. B 116, 2012, 9595−9603

30 Li, Y., Zhang, X., Cao, D., Self-Assembly of Patterned Nanoparticles on Cellular Membranes: Effect of Charge Distribution, J. Phys. Chem. B 117, 2013, 6733−6740

31 Julkowska, M.M., Rankenberg, J.M., Testerink, C., Methods Mol. Biol., 2013, 1009, 261–271

CHAPTER 3

Centrifugation-based assay for examining nanoparticle–lipid membrane binding and disruption

Published in Analyst, 2014, 139, 973-981

Aihong Xi and Geoffrey Bothun

Department of Chemical Engineering

University of Rhode Island

Kingston, Rhode Island, USA

Corresponding author: Geoffrey Bothun

Department of Chemical Engineering

University of Rhode Island

205 Crawford Hall, Greenhouse Road

Kingston, RI, 02881, USA

Phone: +1-401-874-9518

Email: bothun@egr.uri.edu

3.1 Abstract

Centrifugation-based assays are commonly employed to study protein–membrane affinity or binding using lipid bilayer vesicles. An analogous assay has been developed to study nanoparticle–membrane interactions as a function of nanoparticle surface functionalization, membrane lipid composition, and monovalent salt concentration (NaCl). Anionic (carboxylic acid, Ag–COOH), cationic (amine, Ag–NH), and polyethylene glycol coated (Ag–PEG) silver nanoparticles (AgNPs) were examined based on their surface plasmon resonance (SPR), which was used to determine the degree of binding to anionic, cationic, and zwitterionic membrane vesicles by analyzing supernatant and sediment phases. SPR was also used to examine AgNP aggregation in solution and at membrane–water interfaces, and direct visualization of AgNP–membrane binding, vesicle aggregation, and vesicle disruption was achieved by cryogenic transmission electron microscopy (cryo-TEM). The extent of AgNP binding, based on AgNP + vesicle heteroaggregation, and vesicle disruption was dependent upon the degree of electrostatic attraction. Because of their biological and environmental relevance, Ag–PEG + anionic vesicles systems were examined in detail. Cryo-TEM image analysis was performed to determine apparent membrane–water partition coefficients and AgNP aggregation states (in solution and bound to membranes) as a function of NaCl concentration. Despite possessing a PEG coating and exhibiting a slight negative charge, Ag–PEG was able to bind to model anionic bacterial membranes either as individual AgNPs (low salt) or as AgNP aggregates (high salt). The centrifugation assay provides a rapid and straightforward way to screen nanoparticle–membrane interactions.

3.2 Introduction

Nanoparticles interact with cell membranes by first binding at the membrane–water interface. Interfacial interactions and the adhesive binding strength are based on nanoparticle surface functionalization and membrane lipid composition, and control the extent to which a nanoparticle will penetrate into the membrane and disrupt lipid organization and membrane structure.[1,2] There is evidence that these nanoparticle–membrane interactions inhibit cellular function and contribute to nanoparticle toxicity.[3–6] A number of experimental techniques have been used to study nanoparticle interactions with model cell membranes, which are commonly employed to investigate binding mechanisms and biophysical changes in membrane structure, including atomic force microscopy,[7–9] fluorescence microscopy,[10] quartz crystal microbalance,[11–15] differential or isothermal scanning calorimetry,[16–19] electrical capacitance,[20] and cryogenic transmission electron microscopy.[15, 21, 22] These studies have provided critical information that will be needed to develop approaches that can predict nanoparticle–membrane interactions based on nanoparticle composition, geometry, and physicochemical properties.

Based on the experimental techniques employed, nanoparticle–membrane interaction studies have largely focused on lipid bilayers supported on solid planar or spherical substrates (e.g. microparticles23). While very useful and informative, these systems do not accurately represent an intact cell membrane because they restrict the elastic motion of the bilayer and the capacity for mechanical changes. Given the importance of nanoparticle–membrane interactions in nanotoxicology and nanomedicine, and the vast range in nanoparticle composition, size, shape, and surface

functionalization, there is a need to develop techniques that can rapidly and inexpensively analyze the membrane-activity of nanoparticles using free standing or unsupported membranes. For decades researchers have utilized centrifugation-based assays to determine protein–membrane affinity or binding, where the amount of bound protein can be determined by a mass balance taking into account the supernatant (free protein) and sediment (membrane-bound protein) phases.[24] Proteins are one of nature's nanoparticles, and techniques to examine protein membrane binding are well developed and may be amenable to nanoparticles.

The objective of this work was to test the applicability of a centrifugation-based assay for determining nanoparticle–membrane interactions and to examine electrostatic interactions as a function of nanoparticle and membrane composition. Silver nanoparticles (AgNPs) were examined based on their widespread biological applications (e.g. as antimicrobial agents[6, 25–28]) and relevance to nanotoxicology, and their surface plasmon resonance (SPR) properties.[29, 30] SPR was assessed by ultraviolet-visible (UV-vis) spectroscopy, and the SPR absorbance and wavelength were functions of AgNP concentration and aggregation state. These features were used to determine AgNP concentrations in supernatant and sediment phases, and AgNP aggregation state in solution and after membrane binding. Experiments were conducted using anionic, cationic, and neutral AgNPs and lipid bilayer vesicles as a function of monovalent salt concentration. Unsupported vesicles were used, as in most protein-based assays, to allow for elastic membrane deformation and vesicle destabilization due to nanoparticle binding. Supernatant and sediment phases were characterized by cryogenic transmission electron microscopy (cryo-TEM) to directly image nanoparticle–membrane binding and

to connect changes vesicle stability and structure with the observed centrifugation behavior.

3.3 Materials and methods

3.3.1 Chemicals and materials

1,2-Dipalmitoyl-sn-glycero-3-phosphocholine (DPPC, zwitterionic), 1,2-dipalmitoyl-sn-glycero 3-phospho-(10-rac-glycerol)(DPPG, anionic), and 1,2-dipalmitoyl-3-trimethylammoniumpropane trimethylammoniumpropane (DPTAP, cationic) were purchased from Avanti Polar Lipids (Alabaster, AL). Fig. 3-1A shows the chemical structures of the lipids. AgNPs dispersed in deionized (DI) water were purchased from Ocean Nanotech (Springdale, AR). These included AgNPs (referred to as Ag–PEG) with a monolayer of polyethylene glycol-grafted polyethylenimine (PEI) coating; anionic AgNPs (referred to as Ag–COOH) with a carboxylic acid functionalized amphiphilic polymer coating; cationic AgNPs (referred to as Ag–NH) with a PEI coating (Fig. 3-1C and D). Deionized (DI) ultrafiltered water was obtained from a Millipore Direct-Q3 UV purification system (Billerica, MA) at 18.2 mΩ resistance and pH 6.2. Sodium chloride (NaCl, >99.5%) was purchased from Fisher Scientific (Waltham, MA).

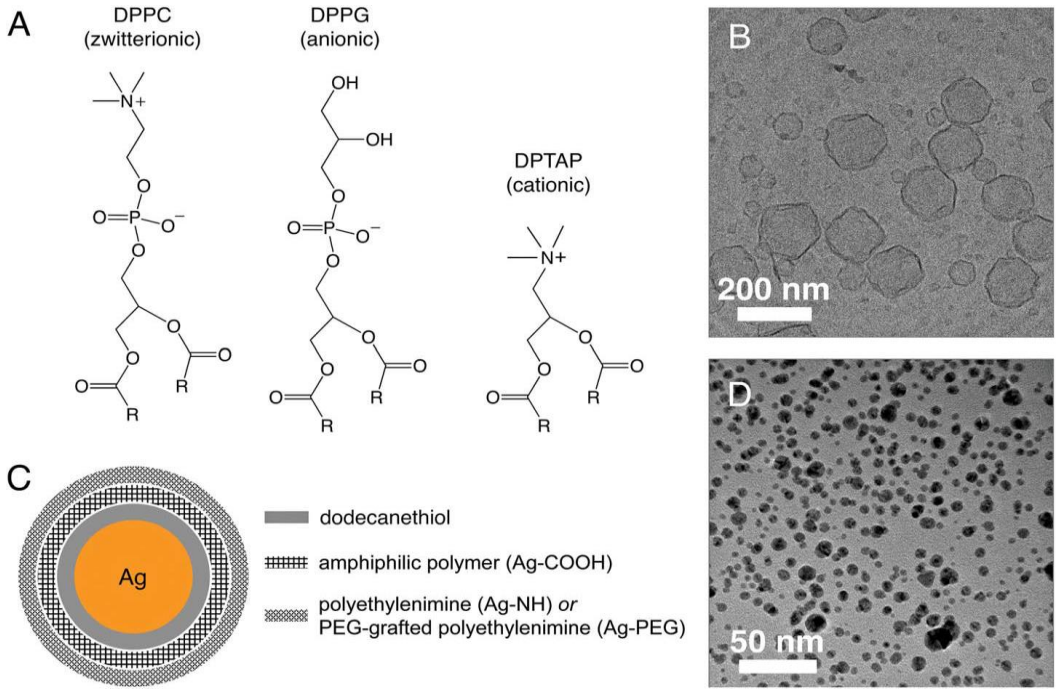

Fig. 3-1 (A) Lipids used to create vesicular model cell membranes. The group, R, represents $C_{15}H_{31}$ acyl tails. (B) Cryo-TEM micrograph of a DPPC/DPPG (3:1) vesicle dispersion. (C) Ag nanoparticle compositions. All nanoparticles studied contain a surface bound dodecanethiol layer. Ag–COOH nanoparticles contain an amphiphilic polymer coating. Ag–NH and Ag–PEG nanoparticles contain an additional PEI or PEG-grafted PEI coating, respectively. (D) TEM micrograph of Ag–PEG nanoparticles.

3.3.2 Membrane (vesicle) preparation

Vesicles were prepared at 10 mM total lipid concentration in DI water or NaCl solutions (10 mM or 100 mM). Lipids, dissolved in chloroform, and water were added to a round-bottom flask, vortexed for 1 min, and then subjected to rotary evaporation at 50 ^{0}C to remove chloroform. After the chloroform was removed, the flask containing vesicles was transferred to a bath sonicator at 50 ^{0}C and sonicated for 30 min. The vesicles were sized by extrusion through double-stacked polycarbonate membranes with 100 nm pore diameters. Neutral membranes were prepared using DPPC and anionic or cationic membranes were prepared using mixtures of DPPC with DPPG or DPTAP at 3 : 1 or 1 : 1 molar ratios, respectively. A representative cryo TEM images of DPPC/DPPG vesicles is shown in Fig. 3-1B.

3.3.3 Cryogenic transmission electron microscopy

Vitrification of sample specimens for cryo-TEM was performed using a Vitrobot (FEI Company), which is a robotic preparation system with controlled temperature and humidity. Specimens were prepared on Quantifoil grids with 2 mm holey-carbon on 200 square mesh copper (Electron Microscopy Sciences, Hat-field, PA). After the sample was equilibrated within the Vitrobot at 25 ^{o}C and 100% humidity for 30 min, the grid was plunged into the sample, withdrawn, and blotted to yield a thin specimen film. The specimen was then vitrified by plunging the grid into liquid ethane, and transferred to liquid nitrogen. Imaging was performed in a cooled stage (model 915, Gatan Inc., Pleasanton, CA) using a JEOL JEM-2100F TEM (Peabody, MA). Image analysis was performed using Image J software.

3.3.4 Dynamic light scattering and zeta potential

Dynamic light scattering (DLS) and zeta potential (z) measurements were performed using a Malvern Zetasizer Nano ZS (Worcestershire, UK) equipped with a backscattering detector angle of 173 and a 4 mW, 633 nm He–Ne laser. Hydrodynamic diameters (d_h) were measured using optical grade polystyrene cuvettes. Results are reported as intensity-weighted z-averages based on 15 consecutive scans. Zeta potential was determined by combined Doppler electrophoretic velocimetry and phase analysis light scattering using folded capillary cells. Zeta potential was computed over 3 cycles (30 data points per cycle) using the Smoluchowski equation.

3.3.5 UV-vis spectroscopy

UV-vis spectroscopy was conducted using an Agilent Cary 50 (Santa Clara, CA) spectrophotometer with a Peltier cuvette holder for temperature control. Samples were equilibrated at 25 ^{o}C for 3 min in quartz cuvettes (10 mm path length) capped with PTFE lids. Absorbance spectra were conducted in triplicate and the SPR peak height, peak area, and peak position (wavelength) of each spectrum was analyzed by OriginPro software (version 9.0).

3.3.6 Centrifugation assay

A schematic of the UV-vis centrifugation assay is given in Fig. 3-2. Vesicles (4 mM) and AgNPs (10, 50, and 100 mg mL^{-1}) were combined in 1 mL samples, magnetically stirred for 3 min, and then kept 25 ^{o}C for 1 h. UV-vis analysis of SPR was conducted on this sample before centrifugation (Fig. 3-2B, solid line 1). The samples

were then transferred to 1.5 mL centrifuge tubes and centrifuged at 6000g for 15 min (Megafuge 16R, Thermo Scientific, Asheville, NC). After centrifugation the sample supernatants, which accounted for approximately 90% of the sample volume, were withdrawn by pipetting and the SPR analyzed by UV-vis (Fig. 3-2B, dash line 2). Supernatant and sediment samples were then analyzed by cryo-TEM. All samples were conducted in triplicate and standard deviations are reported.

Centrifugation conditions were selected after analyzing the sedimentation behavior of the vesicles and AgNPs. The goal was to determine the centrifugation force and time that would not cause vesicle sedimentation, but would lead to the sedimentation of vesicles with bound AgNPs. At 6000g and 15 min vesicles did not sediment consistent with a calculated settling velocity of ~3 x 10^{-4} cm min^{-1} for a 100 nm diameter vesicle based on Stoke's law, which assumes that the vesicles do not interact. However, at this centrifugation condition all three AgNPs exhibited the first signs of sedimentation, and little difference in AgNP sedimentation was observed between DI water and salt solutions (Table S1†).

AgNP binding was inferred based on mass balance obtained by UV-vis analysis of the SPR where SPR peak area was a linear function of AgNP concentration. Apparent AgNP binding was determined as the ratio R_{SPR}

$$R_{SPR} = \frac{\Delta A_{SPR,NPs+vesicles}}{\Delta A_{SPR,NPs}} \quad (1)$$

Where $\Delta A_{SPR,\ NPs+vesicles}$ was the change in the SPR peak area for AgNPs + vesicles before and after centrifugation, and $\Delta A_{SPR,\ NPs}$ was the change for AgNPs. This

approach takes into account the inherent sedimentation behavior of the AgNPs. R_{SPR} = 1 indicated that there was no difference in sedimentation relative to the AgNPs alone.

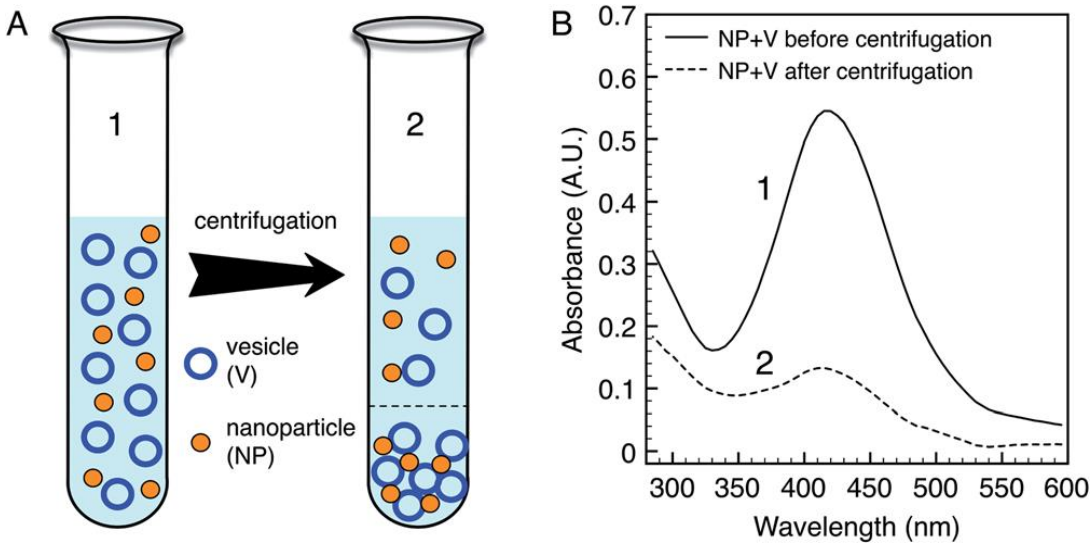

Fig. 3-2 (A) Schematic depicting centrifugation of nanoparticles + vesicles (NP + V) and the boundary between supernatant and sediment phases. (B) Exemplary UV-vis spectra of the AgNP SPR of the supernatant phases before and after centrifugation.

3.4 Result and discussion

3.4.1 Characterization of vesicles and AgNPs

The hydrodynamic diameters and zeta potentials of the AgNPs and vesicles employed are summarized in Tables 3-1 and 3-2, respectively. AgNPs exhibited an average core diameter of 6.4 ± 2.7 nm based on high vacuum TEM analysis and average hydrodynamic diameters from 10–30 nm (Table 3-1). Difference between core and hydrodynamic diameters reflect the polymer coatings. Zeta potential analysis, ζ_{NP}, confirmed the slightly anionic nature of Ag–PEG, and the anionic and cationic nature of Ag–COOH and Ag–NH, respectively. All vesicles exhibited hydrodynamic diameters (d_h) between 95 and 120 nm consistent with membrane extrusion and cryo-TEM analysis (Table 3-2 and Fig. 3-1B). Zeta potentials for charged vesicles, ζ_V, decreased with increasing NaCl concentration consistent with ion binding and charge screening. Based on the average vesicle and AgNP core diameters, the AgNP concentrations examined (10, 50, and 100 μg mL^{-1}) corresponded to approximately 0.4, 2.0 and 4.0 nanoparticles per vesicle (NP : V), respectively, and nanoparticle surface coverage (on the vesicle exterior) ranging from ~0.1% to 7.5%. These ratios were based on vesicles with d_h = 110 nm and an average lipid headgroup area of 0.5 nm^2.[31] The relative strength of the electrostatic attraction or repulsion between vesicles and AgNPs is presented as the product of the zeta potentials, $\zeta_V\zeta_{NP}$, which reflects electrical double layer interactions based on the Poisson–Boltzmann equation (Table 3-2).[32]

Table 3-1. AgNP properties.

	Ag-PEG	Ag-COOH	Ag-NH
Core size (nm)		6.4 ± 2.7	
Hydrodynamic diameter (nm)	19	10	30
Zeta potential[a] (mV)	-16	-45	+57
SPR peak maximum (nm)	410	412	414

[a] Measured in DI water.

Table 3-2. Vesicle (model membrane) properties as a function of lipid composition and NaCl concentration.

Vesicle[a]	NaCl	d_h		ζ_V	$\zeta_V\zeta_{NP}$[b]		
	(mM)	(nm)	PDI	(mV)	Ag-PEG	Ag-COOH	Ag-NH
DPPC	0	120	0.241	<1	<-10	<-29	<+60
DPPC/DPPG (3:1)		95	0.228	-66	+660	+1914	-3960
DPPC/DPPG (1:1)		95	0.231	-72	+720	+2088	-4320
DPPC/DPTAP (3:1)		110	0.195	+60	-600	-1740	+3600
DPPC/DPTAP (1:1)		110	0.172	+70	-700	-2030	+4200
DPPC/DPPG (3:1)	10	110	0.122	-60	+600	1740	-3600
DPPC/DPPG (1:1)		110	0.152	-70	+700	2030	-4200
DPPC/DPPG (3:1)	100	110	0.165	-45	+450	1305	-2700
DPPC/DPPG (1:1)		110	0.148	-50	+500	1450	-3000

[a]Lipid ratio shown in parentheses.

[b]Product of vesicle and AgNP zeta potentials.

3.4.2 Centrifugation assay

R_{SPR} results for Ag–PEG, Ag–COOH, and Ag–NH vesicle binding are shown in Fig. 3-3. For zwitterionic DPPC vesicles, the greatest sedimentation was observed with

Ag PEG, which exhibited a slight negative charge. Little sedimentation was observed with Ag–COOH and Ag–NH. For anionic DPPC/DPPG vesicles, AgNP binding was driven by electrostatic attraction. Ag–PEG and Ag–COOH led to minimal sedimentation due to electrostatic repulsion, while cationic Ag–NH led to near complete sedimentation ($R_{SPR} > 5$) at all NP : V ratios. Increasing the DPPG content within the vesicles (increasing anionic membrane charge) did not affect the sedimentation behavior, which indicates that all Ag–NH nanoparticles bound to DPPC/DPPG vesicles at a 3 : 1 lipid ratio, and that increasing the anionic DPPG concentration did not increasing AgNP binding. This is consistent with the low NP : V ratios examined. For cationic DPPC/DPTAP vesicles, like charged Ag–NH exhibited no binding, which is also consistent with electrostatic repulsion. Anionic Ag–COOH bound completely and led to near complete sedimentation, analogous to that for DPPC/DPPG with oppositely charged Ag–NH. Ag–PEG also bound and caused sedimentation due to its slight negative charge. Sedimentation results from the centrifuge assay correlate with electrostatic double layer attraction (Fig. 3-3D). Results for dioleoylphosphatidylcholine / dioleoylphosphatidylglycerol (DOPC/DOPG) vesicles show that the assay is suitable for fluid phase membranes as well as gel phase (DPPC/DPPG) membranes (Fig. 3-4).

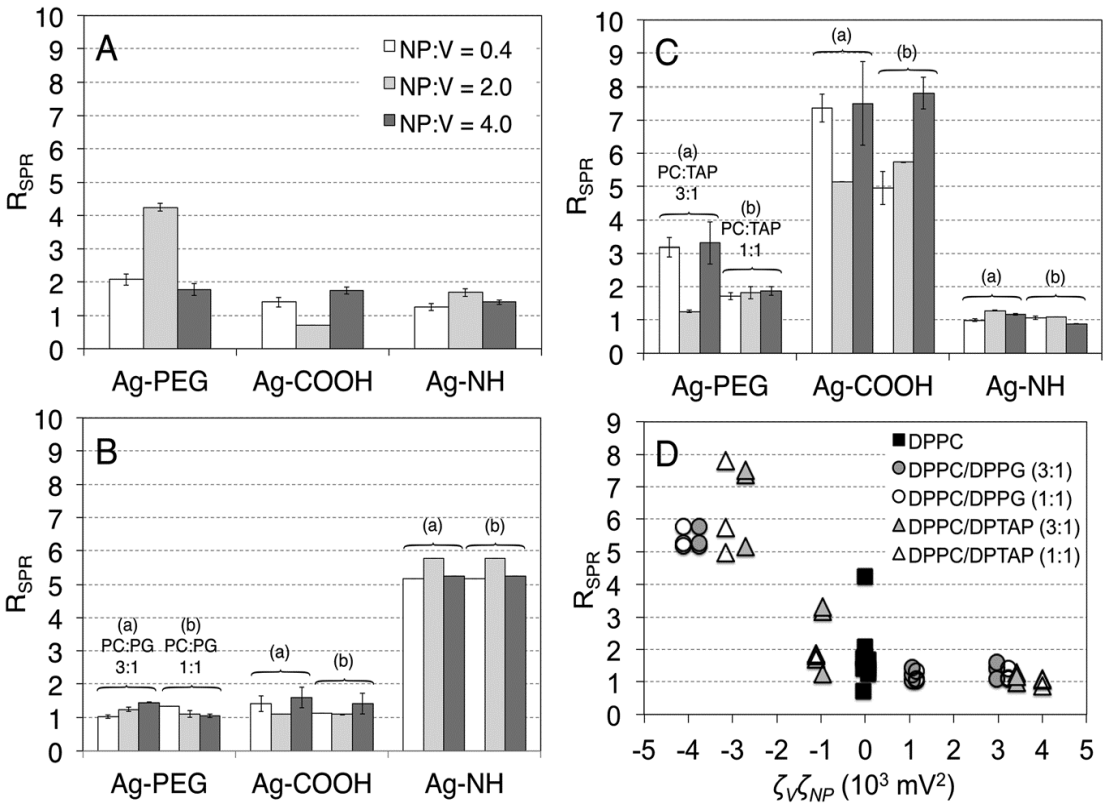

Fig. 3-3 Ratio of the SPR absorbance before and after centrifugation, R_{SPR}, for AgNPs added to (A) DPPC, (B) DPPC/DPPG, and (C) DPPC/DPTAP vesicles in DI water as a function of the nanoparticle to vesicle ratio, NP : V. R_{SPR} takes into account the sedimentation behavior of the nanoparticles alone. Vesicles alone did not sediment at the conditions employed. (D) Correlation between R_{SPR} and AgNP–vesicle electrostatic attraction represented as $\zeta_V \zeta_{NP}$ (Table 3-2).

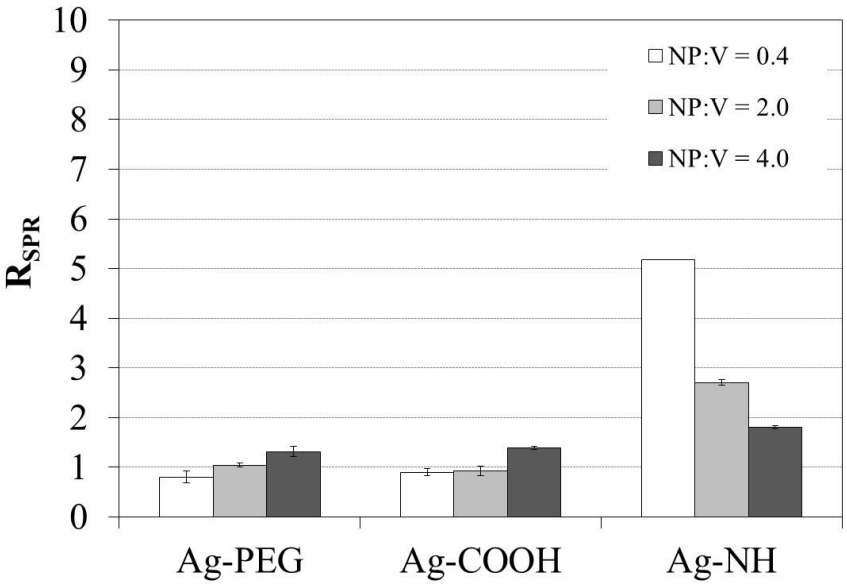

Fig. 3-4 Ratio of the SPR absorbance before and after centrifugation, R_{SPR}, for AgNPs added to DOPC/DOPG (3:1) vesicles in DI water as a function of the nanoparticle to vesicle ratio, NP : V.

DLS measurements were performed on the sample mixtures before and after centrifugation (Fig. 3-5). Strong AgNP binding increased the vesicle hydrodynamic diameter from ~100 nm to >300 nm due to heteroaggregation. After centrifugation the vesicle hydrodynamic diameter within the supernatant returned to ~100 nm, reflecting unbound or unaggregated vesicles. The DLS spectra for like charged AgNPs and vesicles showed no change from the original vesicle suspension.

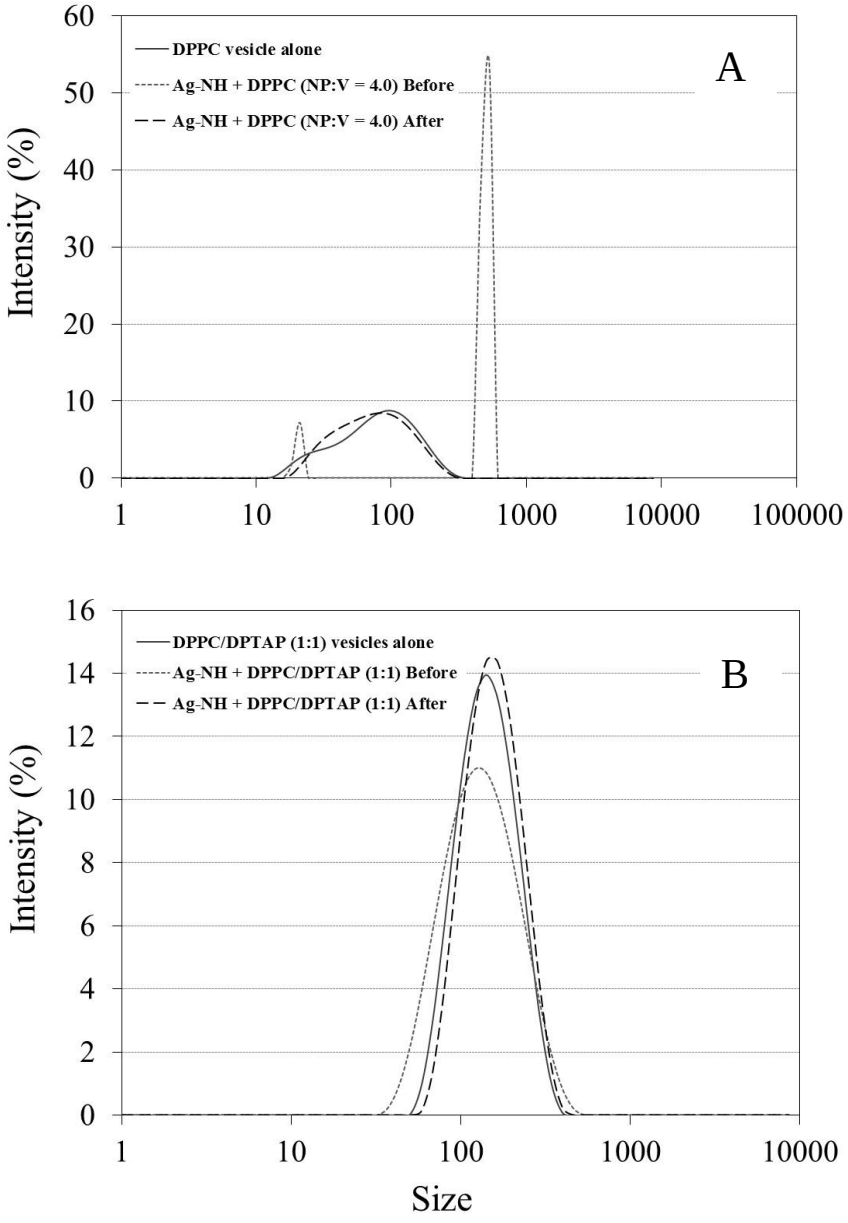

Fig. 3-5 Size distribution of vesicles alone, before centrifugation and after centrifugation. (A) DPPC + Ag-NH, (B) DPPC/DPTAP (1:1) + Ag-NH in DI water at vesicle ratio, NP : V = 4.0.

It should be noted that nanoparticles can bind to lipid vesicles without causing sedimentation. For example, Zhang and Granick[33, 34] have shown that bound anionic and cationic nanoparticles can actually stabilize suspensions of zwitterionic vesicles through electrostatic interparticle repulsion. Similar observations were reported by Chen et al.[21] for small anionic nanoparticles and DPPC/DPTAP vesicles where nanoparticle binding did not lead to vesicle aggregation. These results were obtained at higher nanoparticle surface coverage than this work (e.g. ~25+%), but the phenomenon may still be applicable and could account for some of the anomalous trends in R_{SPR} with AgNP concentration (e.g. Ag–COOH binding to DPPC/DPTAP (3 : 1) vesicles). Hence, while R_{SPR} does account for sedimentation due to strong electrostatic attraction, it is not directly indicative of the extent of nanoparticle binding. As shown in the subsequent sections, vesicles containing bound AgNPs were observed in the supernatant phase even when significant sedimentation occurred.

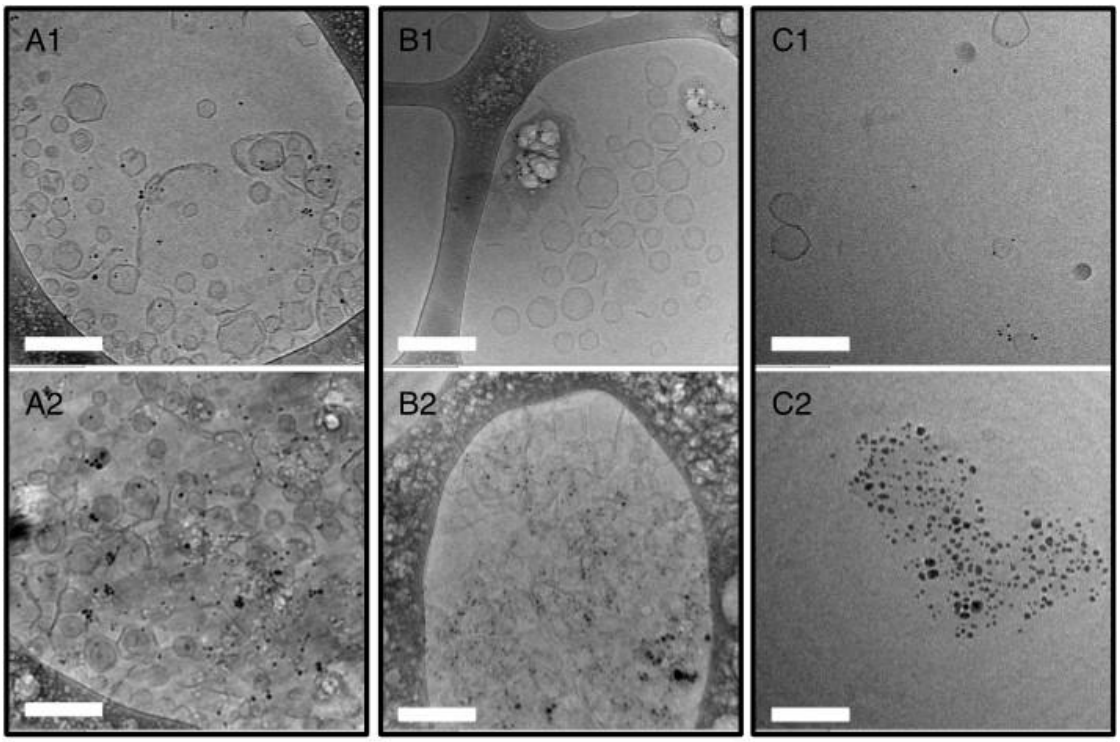

Fig. 3-6. Cryo-TEM micrographs of (A) DPPC + Ag-PEG, (B) DPPC/DPPG (3:1) + Ag-NH, and (C) DPPC/DPTAP (3:1) + Ag-COOH. The NP:V ratio was 3.28. A1, B1, and C1 denote the supernatants and A2, B2, and C2 denote the sediments. The scale bars represent 200 nm.

3.4.3 Cryo-TEM analysis

AgNP–vesicle binding, vesicle structure, and aggregate state were examined by cryo-TEM. The criteria for confirming AgNP binding based on the micrographs was the colocalization of AgNPs and vesicles, AgNPs adopting membrane curvature, and local changes in membrane curvature due to AgNP binding. Micrographs of supernatant and sediment phases are shown in Fig. 3-6 for systems that exhibited the highest binding or R_{SPR} (Fig. 3-6A, DPPC + Ag–PEG; Fig. 3-6B, DPPC/DPPG + AgNH; Fig. 3-6C,

DPPC/DPTAP + Ag–COOH). The supernatants are denoted with a 1 and the sediments with a 2. For DPPC + Ag–PEG, 83 AgNPs were observed in the supernatant with 85% being bound to vesicle surfaces (A1). AgNPs were bound as individual particles and as particle aggregates, and there is evidence of vesicle disruption (opened vesicles and bilayer sheets) due to AgNP binding. These structures were not observed in vesicle samples without AgNPs. Within the sediment (A2), there are more AgNP aggregates, vesicle aggregates bridged by AgNPs, and ruptured and deformed vesicles.

AgNP binding and vesicle deformation was more prevalent for oppositely charged AgNPs and vesicles where all AgNPs were vesicle-bound (no unbound AgNPs were observed). Cationic Ag–NH bound strongly to anionic DPPC/DPPG (3 : 1), leaving unbound vesicles in the supernatant (B1) and completely disrupted vesicles aggregates with bound AgNPs in the sediment (B2). There were some ruptured or deformed vesicles in the supernatant with bound AgNPs (B1), and these regions show damage (melting) of the vitrified sample film due to what it is believed to be local heating of AgNPs by the electron gun. Analysis of this system without centrifugation shows that changes in vesicle structure were driven by AgNP binding and were not simply an artifact of centrifugation. Strong binding was also observed between Ag–COOH and DPPC/DPTAP (3 : 1). Free vesicles and vesicles with bound AgNPs were observed in the supernatant, while large AgNPs and AgNP aggregates are observed in the sediment with completely ruptured vesicles that formed bilayer sheets. Vesicle rupture can be attributed to strong adhesive forces that increase with electrostatic attraction and cause the membrane to partially wrap around or engulf the particle.[35]

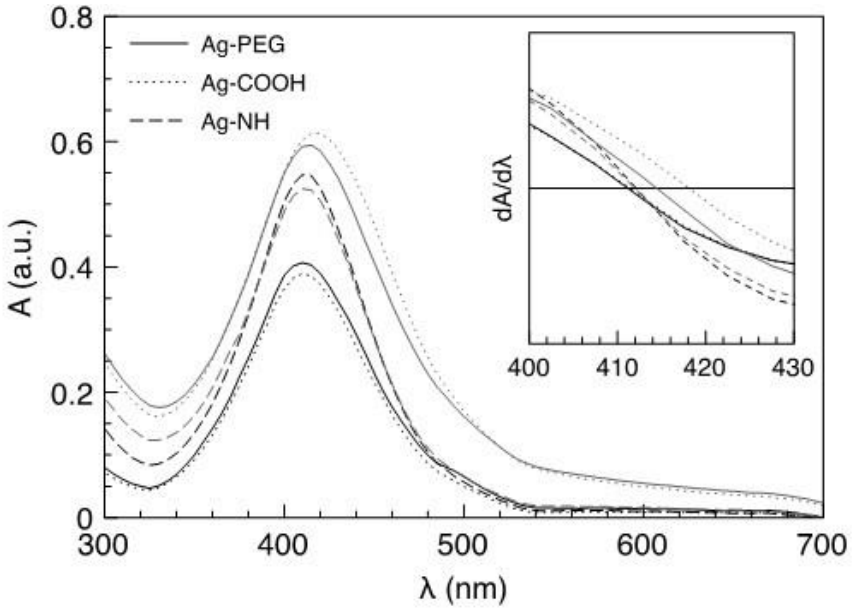

Fig. 3-7. Surface plasmon resonance (SPR) of Ag nanoparticles with PEG (solid lines), COOH (dotted lines), and NH (dashed lines) coatings alone (black lines) or in the presence of DPPC/DPTAP (3:1) (grey lines). The inset shows the derivative of absorbance with respect to wavelength with the horizontal line at $dA/d\lambda = 0$. Measurements were taken before centrifugation.

3.4.4 AgNP binding and aggregation

Cryo-TEM results are consistent with those in Fig. 3-3. Oppositely charged nanoparticles strongly interact with and bind to vesicles, leading to vesicle aggregation and disruption. There was also evidence that AgNP binding led to nanoparticle aggregation at the membrane–water interface. Shifts in the SPR, $\Delta\lambda_{SPR}$, which are sensitive to AgNP size, aggregation state, and surface functionalization, and the presence of adsorbed molecules,[36–39] were examined to investigate this further. Fig. 3-7 demonstrates this analysis for DPPC/DPTAP (3 : 1) vesicles where the SPR for AgNPs

are compared to AgNP + vesicle mixtures before centrifugation **(**$\Delta\lambda_{SPR} = \lambda_{SPR,\ NP+V} - \lambda_{SPR,\ NP}$). All shifts in SPR were 'red-shifts' (Table 3-3) and correlated with electrostatic AgNP–vesicle attraction (Table 3-2). For DPPC/DPTAP, $\Delta\lambda_{SPR}$ was 6.8 nm with Ag–COOH. No change was observed when like charged Ag NH was examined. Similar results were observed for DPPC/DPPG (3 : 1). Interestingly, DPPC showed modest peak shifts with three AgNPs. This may be due to the absence of electrostatic attraction, leaving short-range van der Waals attraction. The SPR shifts could reflect changes in surface functionalization due to lipid adsorption. However, based on the observed aggregation behavior after membrane binding, the $\Delta\lambda_{SPR}$ are consistent with interparticle coupling due to particle clustering or aggregation.[37, 40, 41] Red shifts in $\Delta\lambda_{SPR}$ have also observed for small gold nanoparticle aggregates adsorbed on the surface of larger silica nanoparticles.[42]

Table 3-3. Shifts in the position of the SPR peak, $\Delta\lambda_{SPR} = \lambda_{SPR,\ NP+V} - \lambda_{SPR,\ NP}$, as a function of Ag nanoparticle coating and vesicle composition in DI water.

	$\Delta\lambda_{SPR}$ (nm)		
	DPPC/DPTAP[a]	DPPC/DPPG[a]	DPPC
Ag-PEG	3.6	1.0	1.3
Ag-COOH	6.8	0.6	1.6
Ag-NH	0.1	2.1	0.9

[a]DPPC:DPTAP and DPPC:DPPG ratios of 3:1

3.4.5 Effect of salt concentration

Electrostatic interactions were further probed by varying salt concentration. The studies focused on anionic DPPC/DPPG (1 : 1), which represents a model bacterial membrane, Ag–PEG nanoparticles, and monovalent NaCl. Ag–PEG was selected because PEG coatings are commonly employed in nanomedicine and provide a protective coating that resists protein adsorption.[43–45] In conjunction with centrifugation results (R_{SPR}, Fig. 3-8A), cryo-TEM micrographs were analyzed (Fig. 3-8B and C) to determine apparent AgNP membrane–water partition coefficients, *K*, and to compare the aggregate number for bound and unbound AgNPs (Fig. 3-8D). *K* was calculated as the ratio of bound to unbound AgNPs. This analysis was conducted on supernatant phases and calculated *K* and aggregate numbers were based on a minimum of seven micrographs. Little change in R_{SPR}, *K*, or aggregation number were observed when NaCl concentration was increased from 0 to 10 mM, however clear increases were observed from 10 mM to 100 mM (Fig. 3-8A and D).

Cryo-TEM micrographs depict the effects of salt on *K* and aggregation number. At 10mMNaCl small AgNPs are membrane bound with little evidence of AgNP aggregation in the supernatant. Bound and free AgNP aggregates were observed in the sediment. Close up images show an aggregate closely associated with the membrane (B3) and individual AgNPs causing local changes in membrane curvature (B4). At 100 mM, all AgNPs were present as individual or bound aggregates in the supernatant (C1) and K was ~1, denoting an even distribution of AgNPs between the aqueous phase and the membrane. Aggregates were also observed bound to vesicles in the sediment (C2) and significantly distorting the membranes (C3). Ag PEG binding to DPPC/DPPG

membranes resembles what has been observed for Escherichia coli membranes and anionic (Daxad 19 coated) AgNPs.[27]

AgNP aggregation behavior was further examined by $\Delta\lambda_{SPR}$ for Ag–PEG and Ag–NH particles alone (water and salt) and mixed with DPPC/DPPG (1 : 1) vesicles prior to centrifugation (Table 3-4). Ag–PEG alone exhibited a $\Delta\lambda_{SPR}$ of 1.8 nm at 100 mM NaCl. No change was observed in DI water or 10 mM NaCl, consistent with the results above. In AgNP + vesicle mixtures, Ag–PEG exhibited $\Delta\lambda_{SPR}$ in DI water, but not in salt solution. This suggests that Ag–PEG aggregated at high salt conditions and bound to membranes in the aggregated state. Ag–PEG aggregation also increased its sedimentation rate, but this was accounted for in the R_{SPR} calculation. Comparatively, Ag–NH alone showed no $\Delta\lambda_{SPR}$ due to strong electrostatic repulsion. Only when Ag–NH were added to vesicles did they exhibit a SPR peak shift ($\Delta\lambda_{SPR} > 2$). Unlike Ag–PEG, aggregation of cationic Ag–NH occurred as a result of binding to anionic membranes, and was facilitated by charge neutralization.

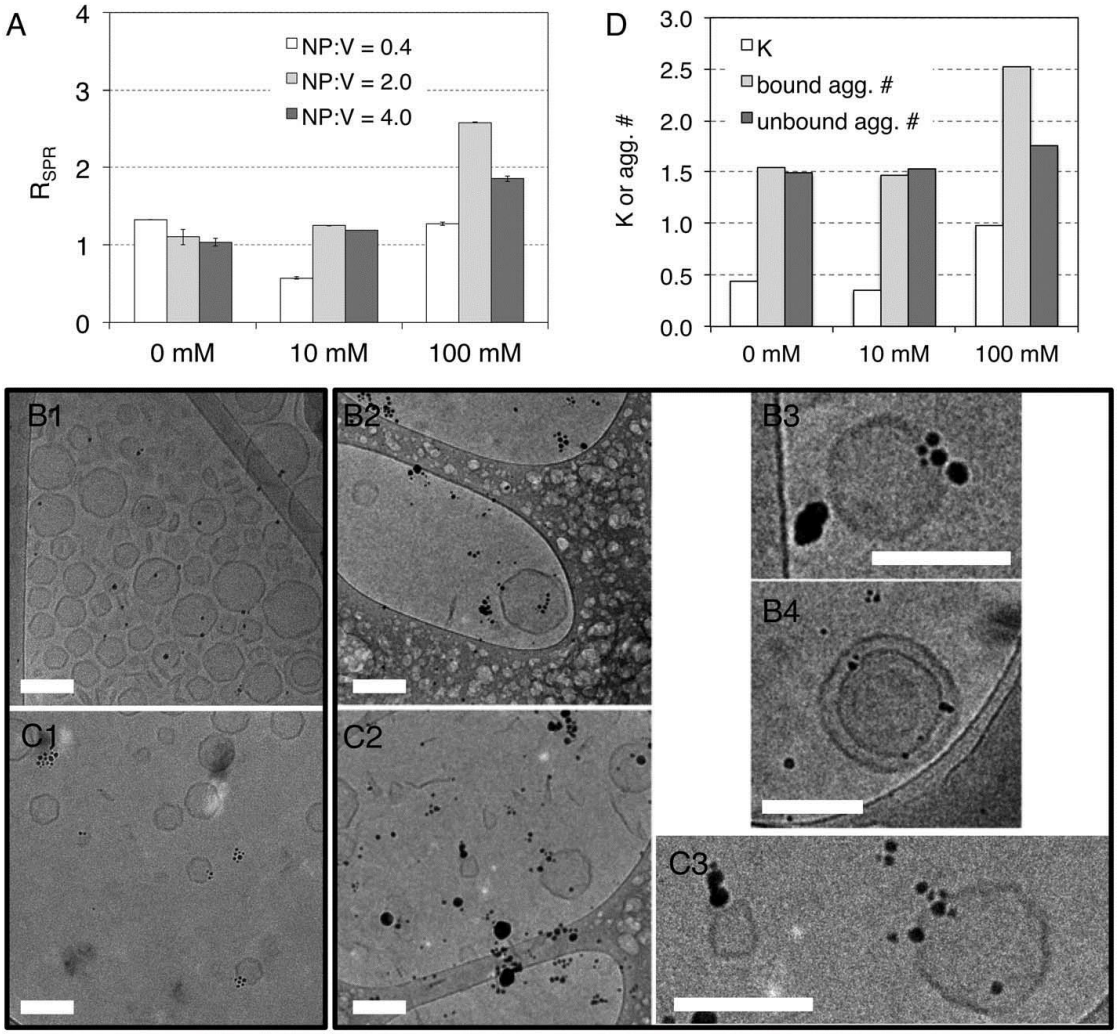

Fig. 3-8. (A) R_{SPR} for DPPC/DPPG (1:1) + Ag-PEG as a function of NaCl concentration. Cryo-TEM micrographs are shown at (B) 10 mM and (C) 100 mM NaCl for the supernatant (B1, C1) and the sediment (B2-B4, C2-C3) phases. Cryo-TEM analysis was conducted at a NP:V ratio of 4.0. The scale bars represent 200 nm. (D) Apparent partitioning coefficients (*K*) and aggregate numbers of vesicle-bound and unbound Ag-PEG nanoparticles as a function of NaCl concentration. *K* and the aggregate numbers were determined within the supernatants after centrifugation.

Table 4. Shifts in the position of the SPR peak as a function of Ag nanoparticle coating and NaCl concentration in DI water.

	$\Delta\lambda_{SPR}$ (nm)			
	NP[a]		NP+V[b]	
NaCl (mM)	Ag-PEG	Ag-NH	Ag-PEG	Ag-NH
0	< 0.1	< 0.1	1.0	2.1
10	< 0.1	< 0.1	0.1	2.6
100	1.8	< 0.1	< 0.1	2.5

[a] $\Delta\lambda_{SPR} = \lambda_{SPR,\ NP\ salt} - \lambda_{SPR,\ NP\ DI}$

[b] $\Delta\lambda_{SPR} = \lambda_{SPR,\ NP+V\ salt} - \lambda_{SPR,\ NP\ salt}$

3.4.6 DLVO analysis

Biological forces play important roles in nanoparticle-membrane interaction. In aqueous solutions, van der Waals (VDW) and double layer electrostatic forces act together to determine whether an interaction is attractive, repulsive or weakly attractive at some finite separation. These two forces are known as the two forces of the Derjaguin-Landau-Verwey-Overbeek theory (the DLVO theory). Understanding biological forces helps to reveal the physical basis of the interactions.

AgNP binding to DPPC/DPPG vesicles was analyzed by DLVO theory where the total interaction energy between an AgNP and a vesicle (V) is the sum of the van der Waals (V_{vdW}) and electrostatic (V_{elec}) interactions. V_{vdW} was calculated as

$$\frac{V_{vdw}}{kT} = \frac{A_{132}}{6kT}\left(\frac{2\,R_1R_2}{h^2+2R_1\,h+2R_2\,h} + \frac{2R_1R_2}{h^2+2R_1h+2R_2h+4R_1R_2} + In\,\frac{h^2+2R_1h+2R_2h}{h^2+2R_1h+2R_2h+4R_1R_2}\right) \quad (2)$$

where A_{132} is the effective Hamaker constant based, R are radii, k is the Boltzmann constant, T is temperature, and h is the surface separation distance based on d_h. Subscripts 1, 2, and 3 denote the AgNP, vesicle, and water, respectively. A_{132} was estimated from the Hamaker constants of the membrane (A_{11}, 8 x 10^{-20} J), water (A_{33}, 3.7 x 10^{-20} J), and the AgNP (A_{22}, 7.2 x 10^{-20} J).

$$A_{132} = \left(A_{33}{}^{0.5} - A_{11}{}^{0.5}\right)\left(A_{33}{}^{0.5} - A_{22}{}^{0.5}\right) \quad (3)$$

Given that the AgNPs contained a thick polymer coating, A_{22} for polyethylene glycol was used.[46] Velec was calculated as

$$\frac{V_{elec}}{kT} = \frac{4\pi\varepsilon_r\varepsilon_0\Phi_1\Phi_2}{kT}\left(\frac{R_1R_2}{R_1+R_2}\right) In\,[1 + exp(-kh)] \quad (4)$$

where ε_r is the dielectric constant of water, ε_0 is the permittivity of free space, Φ are the surface potentials (taken as ζ in DI water), and k is the inverse Debye length. In DI water, k was based on the Na^+ counterion concentration of DPPG (4 mM), and this concentration was added to the 10 and 100 mM NaCl solutions (Fig. 3-9).

For DPPC/DPPG + Ag–PEG, an energy barrier exists near h = 0.5 nm due to electrostatic repulsion. This barrier decreases with increasing NaCl concentration due to charge screening, consistent with the increasing R_{SPR} observed in Fig. 3-8. While this barrier did hinder Ag–PEG binding, it did not prevent it based on the cryo-TEM results. For DPPC/DPPG + Ag–NH, strong electrostatic attraction was observed at all NaCl concentrations despite charge screening. This analysis explains why there was little

change in RSPR with Ag–NH in salt solution.

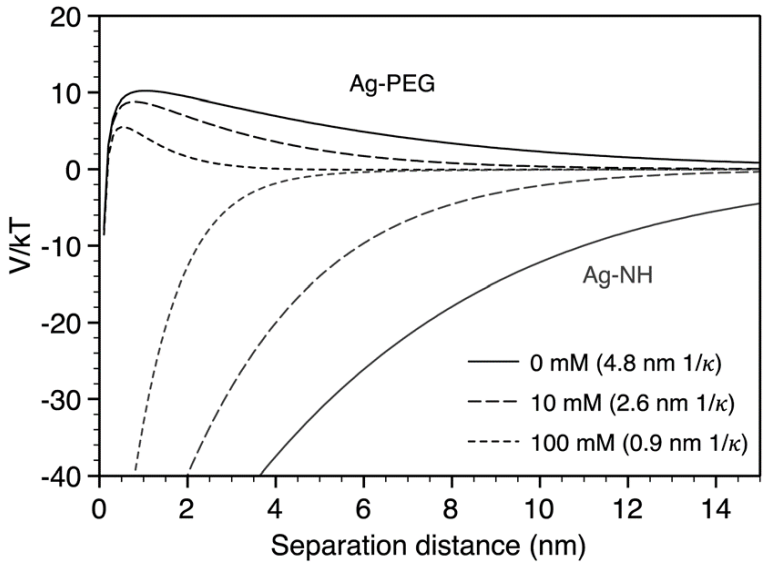

Fig. 3-9 Interaction potential, expressed as *V/kT*, between Ag–PEG or Ag–NH particles and DPPC/DPPG vesicles (1 : 1) as a function of Surface separation distance. NaCl concentrations and the Debye lengths are shown in the legend. For 0 mM NaCl, the Na+ counterion concentration (4 mM) associated with DPPG was used to determine 1/*k*.

3.5. Conclusion

A UV-vis based centrifugation assay, coupled with cryo-TEM and DLS analysis, was introduced as a method for examining nanoparticle–membrane interactions. In analogous protein–membrane centrifugation assays, one can directly measure bound and unbound protein concentrations. This is not as straightforward for the nanoparticle–membrane assay. As opposed to a direct measurement, the nanoparticle–membrane assay reflects changes in the colloidal stability of a sample due to heteroaggregation that is dependent upon the degree of nanoparticle–membrane binding. AgNP + vesicles systems that exhibited strong electrostatic attraction led to significant sedimentation and vesicle/membrane disruption. In contrast, systems that exhibited minimal or no electrostatic attraction did not show significant changes in sedimentation behavior or membrane disruption. This suggests that additional analysis (e.g. imaging) may be needed in conjunction with this assay when examining weakly interacting vesicle–nanoparticle systems. Further optimization of the assay, including centrifugation conditions, vesicle size, nanoparticle concentration, may also improve the ability to examine such systems.

Collectively, the trends observed for nanoparticle binding and membrane disruption as a function of nanoparticle surface chemistry and lipid composition are consistent with previous studies that have demonstrated nanoparticle binding and deformation in small vesicles,[13] giant unilamellar vesicles,[6, 40] planar bilayers,[4] and lipid monolayers[41]; nanoparticle partitioning to supported lipid bilayers;[20] and nanoparticle binding and leakage from vesicles.[42] By analyzing shifts in SPR wavelength and comparing to cryo-TEM micrographs, it was possible to discern different modes of

modes of AgNP binding; individual AgNP binding followed by aggregation at membrane/water interfaces due to charge neutralization, or aggregate AgNP binding due to aggregation in solution caused by charge screening.

References

1 Dawson, K. A., Salvati, A., Lynch, I., Nanoparticles reconstruct lipids, Nat. Nanotechnol. 2009, 4, 84–85

2 Nel, A.E., Madler, L., Velegol, D., Xia, T., Hoek, E.M., Somasundaran, P., Klaessig, F., Castranova V., Thompson, M., Understanding biophysicochemical interactions at the nano–bio interface, Nat. Mater., 2009, 8, 543–557

3 Wu, Y. L., Putcha, N., Ng, K. W., Leong, D. T., Lim, C. T., Loo, J. S. C., Chen, X. D., Biophysical Responses upon the Interaction of Nanomaterials with Cellular Interfaces, Accounts of Chem Reasearch, 2012, Vol. 46, No. 3 ’ 2013 ’ 782–791

4 Sanchez, V.C., Jachak, A., Hurt R.H., Kane, A.B., Biological Interactions of Graphene-Family Nanomaterials: An Interdisciplinary Review, Chem. Res. Toxicol., 2012, 25, 15–34

5 Soenena, S.J., Rivera-Gil b,P., Montenegrob,J.M., Parakb,W.J., De Smedta,S.C., Braeckmansa,K., Cellular toxicity of inorganic nanoparticles: Common aspects and guidelines for improved nanotoxicity evaluation, Nano Today (2011) 6, 446—465

6 Marambio-Jones, C., Hoek, E.M.V., A review of the antibacterial effects of silver nanomaterials and potential implications for human health and the environment , J. Nanopart. Res., 2010, 12, 1531–1551

7 Vasir, J.K., Labhasetwar, V., Quantification of the force of nanoparticle-cell membrane interactions and its influence on intracellular trafficking of nanoparticles / Biomaterials 29 (2008), 4244–4252

8 Xiao, X. Y., Montaño, G. A., Thayne L. Edwards, T. L., Allen, A., Achyuthan, K. E., Ronen Polsky, R.,Wheeler, D. R., and Susan M. Brozik, S. M., Surface Charge Dependent Nanoparticle Disruption and Deposition of Lipid Bilayer Assemblies, Langmuir 2012, 28, 17396−17403

9 Spurlin, T.A., Gewirth, A.A., Effect of C60 on Solid Supported Lipid Bilayers Nano Lett., 2007, 7, 531–535

10 Li S., Malmstadt, N., Deformation and poration of lipid bilayer membranes by cationic nanoparticles Soft Matter, 2013, 9, 4969–4976

11 Frost, R., Jönsson, G. E., Chakarov, D., Svedhem, S., Kasemo, B., Graphene Oxide and Lipid Membranes: Interactions and Nanocomposite Structures, Nano Lett. 2012, 12, 3356−3362

12 Reimhult, E., Za¨ch, M., Ho¨o¨k, F., Kasemo, B., A Multitechnique Study of Liposome Adsorption on Au and Lipid Bilayer Formation on SiO2, Langmuir 2006, 22, 3313-3319

13 Wang, K.F., Nagarajan, R., Mello, C.M., Camesano, T.A., Characterization of Supported Lipid Bilayer Disruption By Chrysophsin-3 Using QCM-D J. Phys. Chem. B, 2011, 115, 15228–15235

14 Eriksson, A.I.K., Edwards, K., Hagfeldt, A., Hernandez, V. A. Physicochemical Characterization of Phosphopeptide/Titanium Dioxide Interactions Employing the Quartz Crystal Microbalance Technique, J. Phys. Chem. B, 2013, 117, 2019–2025

15 Yi, P., Chen, K.L., Influence of Surface Oxidation on the Aggregation and Deposition Kinetics of Multiwalled Carbon Nanotubes in Monovalent and Divalent Electrolytes Environ. Sci. Technol., 2013, 47, 5711–5719

16 Chen, Y.J., Bothun, G.D., Cationic Gel-Phase Liposomes with “Decorated” Anionic SPIO Nanoparticles: Morphology, Colloidal, and Bilayer Properties, Langmuir, 2011, 27, 8645–8652

17 Bhattacharya, S., Srivastava, A., Synthesis and Characterization of Novel Cationic Lipid and Cholesterol-Coated Gold Nanoparticles and Their Interactions with Dipalmitoylphosphatidylcholine Membranes, Langmuir, 2003, 19, 4439–4447

18 Wang, B., Zhang, L.F., Bae, S.C., Granick, S., Nanoparticle-induced surface reconstruction of phospholipid membranes, Proc. Natl. Acad. Sci. U. S. A. 2008, 105, 18171–18175

19 Kelly, C.V., Liroff, M.G., Triplett, L.D., Leroueil, P.R., Mullen, D.G., Wallace, J.M., Meshinchi, S., Baker, J.R., Orr, B.G., Holl, M.M.B., Stoichiometry and Structure of Poly(amidoamine) Dendrimer−Lipid Complexes ACS Nano, 2009, 3, 1886–1896

20 Carney, R.P., Astier, Y., Carney, T.M., Voı̈tchovsky, K., Paulo H. Jacob Silva, P.H., Stellacci, F., Electrical Method to Quantify Nanoparticle Interaction with Lipid Bilayers, ACS nano, 2013, VOL. 7 NO. 2, 932–942

21 Chen, Y.J., Bothun, G.D., Cationic Gel-Phase Liposomes with "Decorated" Anionic SPIO Nanoparticles: Morphology, Colloidal, and Bilayer Properties, Langmuir, 2011, 27, 8645–8652

22 Bihan, O. L., Bonnafous, P., Marak, L., Bickel, T., Trépout, S., Mornet, S., Felix De Haas, F. D., Talbot, H., Taveau, J. C., Lambert, O., Cryo-electron tomography of nanoparticle transmigration into liposome, Journal of Structural Biology 168 (2009) 419–425

23 Hou, W.C., Moghadam,B.Y., Corredor, C., Westerhoff, P., Posner, J.D., Distribution of Functionalized Gold Nanoparticles between Water and Lipid Bilayers as Model Cell Membranes, Environ. Sci. Technol. 2012, 46, 1869−1876

24 Julkowska, M.M., Rankenberg, J.M., Testerink, C., Liposome-Binding Assays to Assess Specificity and Affinity of Phospholipid–Protein Interactions, Methods Mol. Biol., 2013, 1009, 261–271

25 Ahamed, M., Mohamad S. AlSalhi, M.S., Siddiqui, M.K.J., Silver nanoparticle applications and human health, Clinica Chimica Acta 411 (2010) 1841–1848

26 Xiu, Z. M., Zhang, Q. B., Puppala, H. L., Colvin, V. L., Alvarez, P. J., Negligible Particle-Specific Antibacterial Activity of Silver Nanoparticles, Nano Lett. 2012, 12, 4271−4275

27 Sondi, I., Salopek-Sondi, B., Silver nanoparticles as antimicrobial agent: a case study on E. coli asa model for Gram-negative bacteria Journal of Colloid and Interface Science 275 (2004) 177–182

28 Kim, J.S., Kuk, E., Yu, K.N., Kim, J.H., Park, S.J., Lee, H.J., Kim, S.H., Park, Y.K., Park, Y.H., Hwang, C.Y., Kim, Y.K., Lee, Y.S., Jeong, D.H., Cho, M. H, Antimicrobial effects of silver nanoparticles, J. Nanomed. Nanotechnol., 2007, 3, 95–101

29 Li, W. R.; Xie, X. B.; Shi, Q. S.;, Zeng, H. Y.;, Ou-Yang, Y. S.; Chen, Y. B. Appl Microbiol Biotechnol. 2010, 85(4), 1115-22

30 Lubick, N. Environ. Sci. Technol., 2008, 42 (23), p 8617

31 Nagle, J. F., Tristram-Nagle, S., Structure of lipid bilayers, Biochimica et Biophysica Acta, 2000, 1469, 159-195

32 Israelachvili, J., Intermolecular & surface forces, Academic Press, 1991

33 Yu, Y., Anthony, S.M., Zhang, L., Bae, S.C., Granick, S., Cationic Nanoparticles Stabilize Zwitterionic Liposomes Better than Anionic Ones, J. Phys. Chem. C, 2007, 111, 8233–8236

34 Zhang, L.F., Granick, S., How to Stabilize Phospholipid Liposomes (Using Nanoparticles), Nano Lett., 2006, 6, 694–698

35 Li, Y., Zhang, X., Dapeng Cao, D., Self-Assembly of Patterned Nanoparticles on Cellular Membranes: Effect of Charge Distribution, J. Phys. Chem. B 2013, 117, 6733−6740

36 Smith, S. L., Nissamudeen, K. M., Philip, D., Gopchandran, K. G., Synthesis of silver nanoparticles using agar–agar water solution and femtosecond pulse laser irradiationSpectrochim. Acta, Part A, 2008, 71, 186–190

37 Prathna, T. C., Chandrasekaran, N., Mukherjee, A., Biomimetic synthesis of silver nanoparticles by Citrus limon (lemon) aqueous extract and theoretical prediction of particle size, Colloids Surf., A, 2011, 390, 216–224

38 Von White, G., Kerscher, P., Brown, R. M., Morella, J. D., McAllister, W., Dean, D., Kitchens, C. L., Green synthesis of robust, biocompatible silver nanoparticles using garlic extract J. Nanomater., 2012, Article 730746

39 Hotze, E. M., Phenrat, T., Lowry, G. V., Nanoparticle Aggregation: Challenges to Understanding Transport and Reactivity in the Environment J. Environ. Qual., 2010, 39, 1909–1924

40 Ghosh, S. K., Pal, T., Interparticle Coupling Effect on the Surface Plasmon Resonance of Gold Nanoparticles: From Theory to Applications , Chem. Rev., 2007, 107, 4797–4862

41 Mwilu, S. K., El Badawy, A. M., Bradham, K., Nelson, C., Thomas, D., Scheckel, K.G., Tolaymat, T., L. Z. Ma, Rogers, K. R., Smart electrochemical biosensors: From advanced materials to ultrasensitive devices, Sci. Total Environ., 2013, 447, 90–98

42 Westcott, S. L., Oldenburg, S. J., Lee, T. R., Halas, N. J., Formation and Adsorption of Clusters of Gold Nanoparticles onto Functionalized Silica Nanoparticle Surfaces, Chem. Phys. Lett., 1999, 300, 651–655

43 Immordino, M. L., Dosio, F., Cattel, L., Stealth liposomes: review of the basic science, rationale, and clinical applications, existing and potential Int. J. Nanomed., 2006, 1, 297–315

44 Phillips, M. A., Gran, M. L., Peppas, N. A., Targeted nanodelivery of drugs and diagnostics Nano Today, 2010, 5, 143–159

45 Nichols, J. W., Bae, Y. H., Odyssey of a cancer nanoparticle: From injection site to site of action Nano Today, 2012, 7, 606–618

46 Chan, J., Popov, J. J., Kolisnek-Kehl, S., Leaist, D. G., Soret Coefficients for Aqueous Polyethylene Glycol Solutions and Some Tests of the Segmental Model of Polymer Thermal Diffusion J. Solution Chem., 2003, 32, 197–214

47 Sau, T. P., Urban, A. S., Dondapati, S. K., Fedoruk, M., Horton, M. R., Rogach, A. L., Stefani, F. D., Radler, J. O., Feldmann, J., Controlling loading and optical properties of gold nanoparticles on liposome membranes Colloids Surf., A, 2009, 342, 92–96

48 Peetla, C., Labhasetwar, V., Biophysical Interactions with Model Lipid Membranes: Applications in Drug Discovery and Drug Delivery Mol. Pharmaceutics, 2008, 5, 418–429

49 Moghadam, B. Y., Hou, W. C., Corredor, C., Westerhoff, P., Posner, J. D., Distribution of Functionalized Gold Nanoparticles between Water and Lipid Bilayers as Model Cell Membranes, Langmuir, 2012, 28, 16318–16326

CHAPTER 4

CONCLUSION

This study proposes an easy assay analysis to measure surface plasmon resonance R_{SPR} binding and predict interactions of silver nanoparticles with vesicles. R_{SPR} value categorizes three types of binding: oppositely charged particles and vesicles demonstrate destructive interaction, causing vesicles disrupted or totally destroyed. Oppositely charged nanoparticles have strong interactions with vesicles, the binding between nanoparticless and vesicles cause nanoparticle aggregation, and nanoparticle aggregations with vesicles lead to significant sedimentation; similarly charged particles and vesicles show very weak or zero binding, in the between that is moderate binding. Salt concentration does not influence interactions between oppositely charged particles and vesicles because stronger charge maintain nanoparticle stability, however, salt plays significant role for moderate binding of Ag-PEG particles with DPPC/DPPG, higher salt concentration makes nanoparticles aggregate , particles aggregates interact with the vesicles rather than individual particles; nanoparticle aggregates are capable of penetrating into the vesicles and inducing local changes in membrane curvature.

Compared to protein-membrane centrifugation assays, nanoparticle-membrane assays do not allow one to directly quantify the degree of nanoparticle binding or the membrane/water partition coefficient of the nanoparticle. Rather, the nanoparticle-membrane assay reflects the change in the colloidal stability of the vesicle with nanoparticle sample due to nanoparticle-membrane binding. Two aspects are clear,

strong nanoparticle-membrane interactions lead to vesicle aggregation, vesicle disruption/rupture, and nanoparticle aggregation (due to charge neutralization by adsorbed lipids) while weak nanoparticle-membrane interactions do not lead to significant aggregation or vesicle disruption. Centrifugation assisted UV-vis assay provides an inexpensive, useful and quick technique to screen nanoparticle-membrane interaction.